Modelling ecological impacts of metal bioaccumulation from mid-water plume discharges

Project: Integrated Ecosystem Assessment and Ecosystem-Based Management Framework for Polymetallic Nodule Collection Activities

June 2025

Pethybridge H, Fulton EA, Parr JM, Dunstan PK, Rowden AA, Dambacher JM

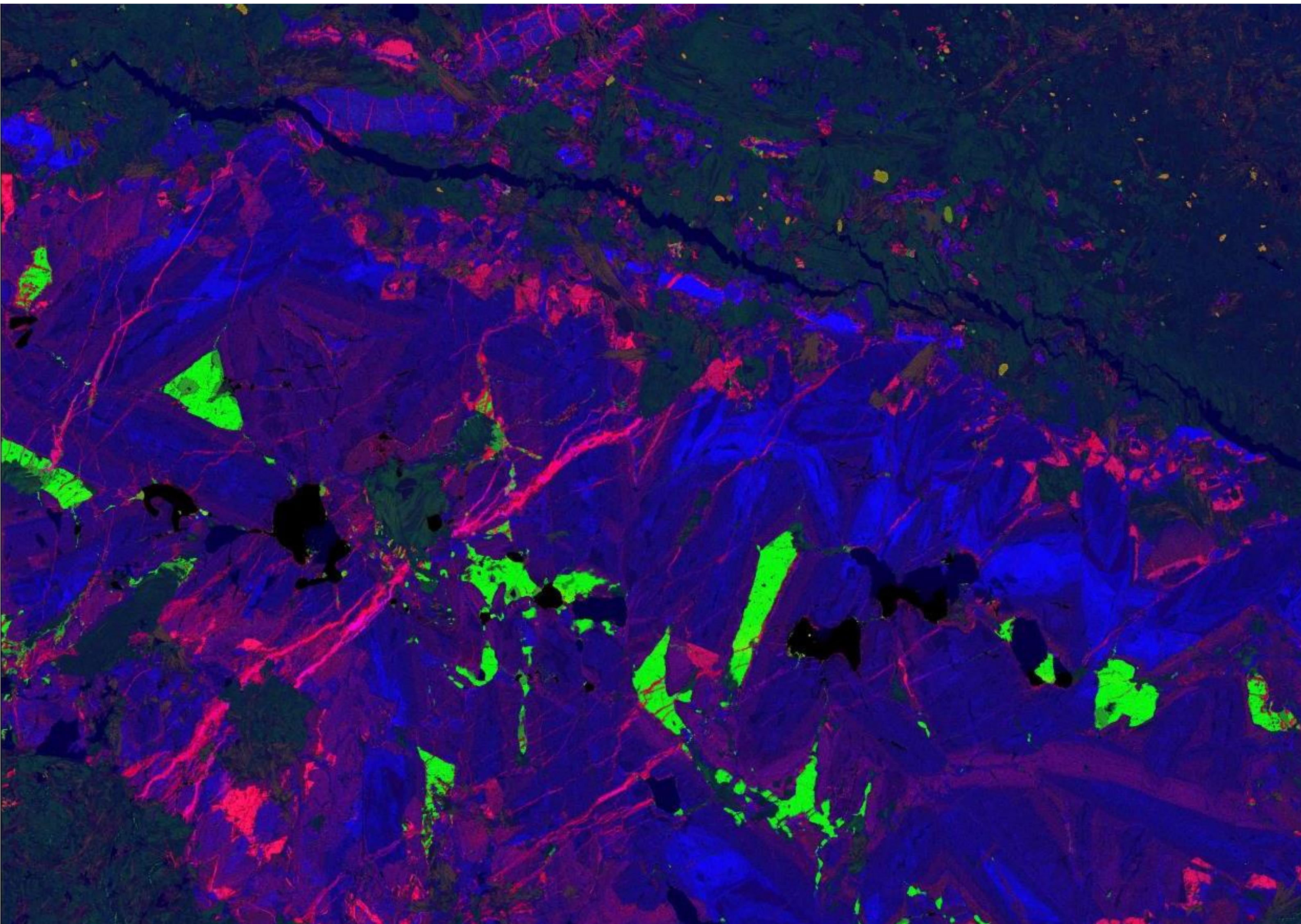

Prepared by the CSIRO Research Consortium for The Metals Company Australia Pty Ltd.

The 2021–2025 consortium, led by CSIRO, includes Museums Victoria, Griffith University, University of the Sunshine Coast and NIWA.

Citation

Pethybridge H, Fulton EA, Parr JM, Dunston PK, Rowden AA, Dambacher JM. 2025. *Modelling ecological impacts of metal bioaccumulation from mid-water plume discharges*. CSIRO Marine Laboratories, Hobart.

Copyright

Important disclaimer

Acknowledgement of Country

CSIRO acknowledges the Traditional Owners of the lands, seas and waters, of the area that we live and work on across Australia and pays its respects to Elders past and present. CSIRO recognises that Aboriginal and Torres Strait Islander peoples have made, and will continue to make, extraordinary contributions to Australian life including in cultural, economic, and scientific domains.

Acknowledgements

The analysis and writing of this report was funded by The Metals Company Australia Pty Ltd through a contract to a research consortium that includes the Commonwealth Scientific and Industrial Research Organisation (CSIRO, Australia), National Institute of Water and Atmospheric Research (NIWA, New Zealand), Griffith University, University of the Sunshine Coast, and Museums Victoria (Australia).

Contents

Figures

Tables

Executive summary

This study developed and applied an ecosystem modelling framework to evaluate potential ecological impacts associated with deep-sea mining midwater discharge plumes in the Clarion-Clipperton Zone (CCZ) region of the Pacific Ocean. Specifically, it examined how mid-water discharge plumes may interact with pelagic biota, including marine mammals and commercially important tunas, through direct exposure and food-web pathways involving vertically migrating mesopelagic communities. The modelling approach involved updates to an existing Ecopath with Ecosim (EwE) food web model for the focal region, including enhanced food web linkages, improved vertical connectivity, and integration of metal bioaccumulation tracing via Ecotracer.

The updated ecosystem model incorporated vertically-distributed functional groups of organisms (epipelagic, mesopelagic, and bathypelagic) and included parameterizations for three representative metal groups with distinct toxicological profiles: (i) highly toxic and persistent metals (*e.g*., mercury, lead and cadmium), (ii) moderately toxic metals (*e.g.*, zinc and nickel), and (ii) biologically active and essential trace elements (*e.g*., iron). A set of scenarios were run simulating discharge plume releases at different depths (200–1,000 m and 1,000–3,000 m), with metals introduced at varying inflow rates representing baseline atmospheric and volcanic input conditions, small concentration increases (baseline +5% and +10%), and extreme concentration increases (baseline +20% and +50%). Sensitivity analyses explored responses to changes in toxicokinetic parameters including initial concentrations and uptake, elimination, and metabolic decay rates.

Key Findings:

- Simulated metal concentrations were found to be impacted by discharge depth, metal type, and trophic level.
- Model-derived Trophic Magnification Factors (TMFs) confirmed clear biomagnification trends among different metal types, ranging from 2.53 (essential trace elements, Metal group 3) to 4.97 (toxic and persistent metals, Metal group 1).
- Long-lived top predators, such as swordfish and large sharks, accumulated the highest simulated metal concentrations, consistent with their trophic position and life-history.
- Mid-water plume discharges at mesopelagic depths (200–1,000 m below surface) led to broader ecosystem exposure, with all consumer groups showing detectable to medium increases in contaminant loadings, remaining below 10% of international health advisory thresholds. This included sharks, tunas, and marine mammals.
- Bathypelagic discharges (1,000–3,000 m) had localised effects, with bioaccumulation largely restricted to deep-dwelling zooplankton and fish. No detectable increases in metal concentrations were observed for epipelagic top-predators such as tunas and marine mammals. Model estimates indicate that discharges below 1,000 m are unlikely to significantly increases contaminant loads in pelagic marine species. Predicted concentrations across all taxa remained well below international health advisory limits.

Implications and recommendations

The modelling results indicate:

- The vertical placement of sediment discharge plumes is a key determinant of ecological impact. Discharges between 1,000 and 3,000 m are more spatially contained, while those shallower than 1,000 m led to broader ecosystem exposure and overlap with species that may already exhibit elevated metal concentrations. Where mid-water discharge is unavoidable, bathypelagic depths (>1,000 m) should be prioritised to minimise contaminant transfer into upper ocean ecosystems.
- The importance of establishing precautionary thresholds for cumulative metal exposure, particularly for high-trophic-level species with long life spans and slower elimination rates.
- The importance of conservative inflow limits, robust baseline monitoring and ongoing model refinement to inform discharge strategies and evaluation.

Future work priorities to support more robust environmental risk assessments via improved model realism should include:

- Vertical and spatial heterogeneity in plume dynamics.
- Improved characterisation of chemical speciation and partial bioavailability of metals, including reducing uncertainties in background environmental concentrations and natural inflow source fluxes, to better constrain exposure and accumulation dynamics.
- Representation of highly mobile species, including ontogenetic and seasonal shifts in distribution and exposure.
- Expanded empirical datasets on metal concentrations across a broader range of taxa groups, including invertebrates and mesopelagic species.
- Clarifying feeding-migration pathways that could transport contaminants from deeper depths up into the meso- and epipelagic zones.

These findings provide a foundational, ecosystem-scale framework for evaluating metal bioaccumulation under varying exposure conditions, supporting spatially-informed impact assessments of potential mid-water sediment plume discharges from deep-sea mining. They underscore the importance of early detection of contaminants in lower trophic levels and the need for vertically-explicit ecological models to inform regulatory frameworks.

1 Introduction

The mining of polymetallic nodules involves removing them from the uppermost layers of the seabed, separating nodules from sediment on ships, and discharging clay-rich sediments and ambient water back into the ocean (Miller *et al*. 2018). This discharge generates sediment plumes that can introduce both nutrients and heavy metals into the water column. Recent research indicates that such mid-water discharges may contribute to increase acidification and oxygen depletion, while also potentially altering key ecological processes such as bioluminescence and feeding behaviour (Christiansen *et al.* 2020). The environmental risks associated with these mid-water plumes remain largely unexplored, particularly regarding their impacts on deep and mesopelagic ecosystems that support pelagic food webs (Drazen *et al.* 2019a; Drazen *et al.* 2020).

Recent studies suggest that climate change may increase spatial overlap between tuna fisheries and proposed deep-sea mining activities in the Clarion-Clipperton Zone (CCZ) of the Pacific Ocean by altering the distribution and behaviour of vertically migrating mesopelagic species (Amon *et al.* 2023). This overlap, driven by projected shifts in tuna (*i.e.*, yellowfin, bigeye, and skipjack) distributions and biomasses, has raised concerns about potential future conflicts as a result of overlapping areas of operations between deep-sea mining and fishing industries (Van Der Grient and Drazen 2021, Amon *et al.* 2022). However, existing research has not specifically examined how plume discharge depth or food web linkages may impact these interactions. The role of mesopelagic communities in shaping the spatial and temporal dynamics of discharge plumes remains unknown.

Mid-water discharge plumes serve as a major potential pathway for mining-derived trace metals and other contaminants to enter pelagic ecosystems (Miller *et al.* 2018). The depth of release of these contaminants, whether in the upper mesopelagic or deeper bathypelagic zones, could significantly affect contaminant bioavailability and subsequent bioaccumulation patterns (Drazen *et al.* 2020). Shallow plume releases (less than 1,000 m) may have greater interactions with epipelagic communities where biodiversity, biomass, and primary production are highest (Robison *et al*. 2010; Choy *et al.* 2017), and where potential overlap with fisheries is greatest, whereas deeper discharges may impact bathypelagic food webs, where slower metabolic rates and distinct trophic pathways govern energy flow.

Ecosystem models provide a tool for evaluating the movement of contaminants through trophic networks (Arnot and Gobas 2004; Rose *et al.* 2010; Ferris and Essington 2014; De Laender *et al.* 2015; Craig and Link, 2023). By integrating complex life-history structures and trophic interactions, these models capture the key processes that govern the fate and transport of metals and other contaminants within ecosystems (Ouillon *et al.* 2022; Stanley *et al.* 2020). Incorporating such dynamics allows for scenario testing across a range of discharge depths and contaminant concentrations. These insights are crucial for supporting evidence-based regulations and environmental management frameworks aimed at reducing potential ecological risks of deep-sea mining.

1.1 Study objectives

The aim of this project was to evaluate the potential for metal bioaccumulation resulting from mid-water discharge plumes associated with deep-sea mining in the NORI-D lease of the CCZ, focusing on how metals may interact with pelagic organisms through food web pathways. To support this, we updated an existing open-ocean ecosystem model representing the CCZ to:

1. Synthesise our understanding of food web linkages within the pelagic, mesopelagic, and bathypelagic zones in the CCZ, with particular attention to vertically migrating species and trophic connectivity.
2. Assess the likely effects of mid-water discharge plumes on pelagic top predators and other functional groups by tracing the transfer and bioaccumulation of different metal compounds potentially made bioavailable through discharges.
3. Conduct scenario testing to evaluate:
    a. Potential for bioaccumulation across a ranges of metal compound types present in discharge plumes. Metals were grouped into three categories based on their toxicity, bioaccumulative potential, and persistence or biologically-activity. These classifications align with those used in regional assessments of baseline and source metal concentrations in the study area which include: (i) potentially hazardous chemicals, and (ii) essential trace-elements (The Collector Test Report: Fitzsimmons *et al.* 2025).
    b. Bioaccumulation potential across modelled functional groups under a range of exposure concentrations, from baseline natural inputs (e.g. atmospheric and volcanic sources) to extreme levels representing upper-bound discharge scenarios designed to test system sensitivity.
    c. Discharge depth, comparing releases in (i) the mesopelagic zone between 200–1,000 m and (ii) the bathypelagic zone (1,000–3,000 m). The model was updated to include enhanced representation of mesopelagic and deep-dwelling fish, squid, and zooplankton. We assumed some trophic transfer from these deeper groups to epipelagic predators, although the ability of species to traverse the oxygen minimum zone remains uncertain and is not explicitly represented in the model.
4. Perform sensitivity analyses and comparative modelling to address parameter uncertainty, including:
    a. Variation in direct uptake rates (*e.g.,* via respiration, osmoregulation, and dermal absorption of soft-bodied organisms).
    b. Changes to initial environmental metal background concentrations.
    c. Changes to elimination (assimilation efficiency) rates.
    d. Structural differences across independently developed oceanic food web models in the Pacific Ocean.
5. Evaluate ecological impacts of mid-water discharge plumes by comparing model-predicted contaminant levels to relevant environmental guideline thresholds for each metal group.

2 Methods

2.1 Ecosystem model, Ecopath with Ecosim

All trophic and metal bioaccumulation simulations were conducted with the Ecopath with Ecosim (EwE) software package (version 6.6.8: https://ecopath.org/). The EwE modelling framework has been extensively applied in regional and global marine systems (reviewed by Keramidas *et al.* 2023) to assess potential trophic impacts of human impacts, physical climate drivers, and management interventions (Christensen *et al.* 2005, Colléter *et al.* 2015; Heymans *et al.* 2016), including multiple stressor effects (Stock *et al.* 2023). In addition to its role in fisheries and food web modelling, EwE has also been adapted for contaminant tracking studies, enabling researchers to investigate the biomagnification and trophic transfer of essential elements (Sandberg *et al.* 2007) and pollutants such as mercury (Ferris and Essington 2014; Li *et al.* 2022), microplastics (McMullen *et al.* 2024), and oils spills (Rohal *et al.* 2020) in marine food webs.

This project utilised two existing EwE models of open ocean ecosystem types within the Pacific Ocean (Table 2-1**Error! Reference source not found.**). That is the Eastern Tropical Pacific Ocean (EwE ETP, Olson and Watters 2003), and the Western Tropical Pacific Ocean (EwE WARM; Godinot and Allain 2003) EwE models. All original models were downloaded from EcoBase, a publicly available repository of published Ecopath models, on 29/11/2023.

Table 2-1. Details of published Ecopath with Ecosim (EwE) models used in this study.

Model name	period	Eco type	Groups	latitude	longitude	Model area (km^2)	depth	reference
ETP (Eastern Tropical Pacific)	1993-1997	Pelagic ocean	39	20N-20S	150W-70.124E	32,800,000	0–1,000	Olson *et al.* 2003
WTPO (Western Tropical Pacific)	1990-2000	Pelagic ocean	20	110W-180E	N15-S15	2.55E+07	0–1,000	Godinot and Allain 2003
ETP updated	2000-2015	Mesopelagic	49	20N-20S	150W-70.124E	32,800,000	0–3,000	This study

Ecosim was used to represent temporal dynamics of functional groups and is a prerequisite for using the Ecotracer routine to estimate flows of a contaminant in the system. While fisheries and biomass time-series data can enhance EwE model calibration, they were not incorporated in this study which centres on contaminant bioaccumulation under a steady-state assumption commonly applied in contaminant-focused models (*e.g.,* Ferris and Essington 2014; McMullen *et al.* 2024). This approach aligns with best practice recommendations to match model complexity to study objectives, particularly when time-series data are not central to the research focus, such as assessments of contaminant fate and trophic transfer (Heymans *et al.* 2016).

The ETP EwE model was selected for updating and primary use in subsequent metal bioaccumulation testing due to its coverage of the CCZ and its focus on tuna. The model represents eight commercially important tuna and billfish species (*i.e.*, yellowfin, bigeye, bluefin, albacore, skipjack, marlin, sailfish and swordfish), with four tuna species further divided into size classes (large and small, as described by Olson and Watters 2003), allowing for a more detailed representation of known diet and biological differences and thus assessment of size-based ecological dynamics. First, biomass units were adjusted for model area (into *t/km²*), followed by pre-balance checks of all input parameters (Link 2010, Heymans *et al.* 2016). The food web matrix was revised with more recent dietary data and understanding of mesopelagic communities and their vertical distributions and migrations. Specifically, we used recent dietary data on tunas (*i.e.,* Dambacher *et al.* 2010; Olson *et al.* 2014; Duffy *et al.* 2017) within the Eastern Tropical Pacific that have also shown decadal, climate driven, shifts in tuna diet from more energetically rich epipelagic prey to smaller mesopelagic species and range expansion of some tuna species (Olson *et al.* 2014).

We extended the vertical distribution of the model from a maximum depth of 1,000 m to 3,000 m to better represent food web dynamics in both the mesopelagic zone (200–1,000 m) and the bathypelagic zone (1,000–3,000 m). To achieve this, we added and parameterised 11 additional functional groups. This addition included representing three groups of mesopelagic fishes: (1) mesopelagic residents (that do not undergo vertical migration), (2) shallow diel vertical migrators (that migrate between the mesopelagic to epipelagic zones from 1,000 m to 0–100 m), and (3) deep diel vertical migrators (that migrate between the bathypelagic and mesopelagic zones just beyond 1,000 m). We also added a bathypelagic fish resident functional group with a habitat between 1,000 to 3,000 m to represent the presence of deep dwelling fishes (Drazen *et al.* 2019). One additional cephalopod, and two additional zooplankton and microzooplankton groups were also included to differentiate those organisms primarily living in the epipelagic (0–200 m), mesopelagic (200–1,000 m) and deeper waters (1,000–3,000 m). Lastly, we included two additional detritus groups so that there was a detritus group for each vertical habitat zone (epipelagic, mesopelagic, and bathypelagic). These changes were necessary to enable the model to explore the release of plumes at deeper midwater depths and capture potential interactions between vertical migrating mid-trophic species and higher-order pelagic species (such as tunas and marine mammals). The inclusion of additional mesopelagic groups enhances the connectivity between the mesopelagic and epipelagic zones, facilitating the vertical transfer of both biomass and contaminants. In contrast, direct transfer from the bathypelagic to the upper ocean layers is limited and occurs through two pathways: (i) the deep vertically migrating mesopelagic fish feeding marginally on deep zooplankton; and (ii) very minor predation on bathypelagic fish by deep-diving pelagic predators. Only two taxa groups were considered capable of diving to bathypelagic depths to feed on these bathypelagic fishes: bigeye tuna (Duffy *et al.* 2017) and toothed whales (Amano and Yoshioka 2003). Variants of the updated ETP EwE model were tested with and without these predator-prey connections. Transfer of mass and contaminants from the epipelagic to bathypelagic zones occurs primarily through passive detrital flux, including the sinking particulate organic matter and faecal pellets. The updated ETP EwE model excluded abyssal and benthic habitats in the CCZ (3,500–5,800 m), as the study focused on impacts from midwater, not benthic, discharge plumes.

To implement the model update, biomass was first partitioned among the new functional groups. Biomasses for all deeper dwelling groups were smaller than equivalent mesopelagic and epipelagic groups as supported by the literature (Irigoien *et al.* 2014), in addition to both trawl and acoustic observations undertaken at the CCZ (Ryan 2024). Alterations, where possible, were based on the parameterisation of functional groups included in other open ocean or deep water Ecopath models (*e.g.,* Choy *et al.* 2016). Slight adjustments to the standard input parameters (*e.g.,* P/B, C/B, EE) of several original groups, including *Auxis* (bullet tuna) and tuna, were made to achieve mass balance, consistent with recommended practices in Ecopath modelling (Christensen *et al.* 2005; Heymans *et al.* 2016). The model produced stable biomasses for most functional groups after five to ten years of simulation. Functional groups that showed gradual increases in relative biomass over the 20-year model run included mesopelagic dolphins (0.5), toothed whales (0.2), skipjack (0.16), albacore (0.13), and large sharks (0.12). Large bigeye and large marlin were the only groups that continued to show declines (0.14) in relative biomass over the model run period. Parameterization and food web representation of the final model are provided in Table 2-2 and Figure 1.

Environmental conditions (*e.g.*, primary productivity) were held constant across all model runs to isolate the effects of metal bioaccumulation on different functional groups under varying exposure scenarios. This approach allowed us to focus on the influence of exposure location and trophic transfer, without confounding effects from environmental variability. As our primary interest was in understanding how bioaccumulation patterns differ in deeper environments, which are typically more stable and less influenced by surface environmental variability, this approach was considered the most appropriate.

Table 2-2. Final parameterization of the updated EwE ETP model. (*) represents newly added functional groups; D – refers to functional groups with some dietary connections to deeper dwelling (>1,000 m) prey items; M – reflects mesopelagic producers and first level consumers inhabiting waters between 200 and 1,000 m, and S refers to surface dwelling (0-200 m) producers and first level consumers.

Group name	Trophic level	Biomass (t/km^2)	P/B (/year)	C/B (/year)	EE	P/C (/year)
Pursuit Birds	4.88	0.0018	0.08	65.70	0.13	0.00
Grazing Birds	3.84	0.0004	0.15	65.70	0.17	0.00
Baleen Whales	3.81	0.0277	0.02	9.10	0.00	0.00
Toothed Whales – D	5.24	0.0945	0.02	6.75	0.00	0.00
Spotted Dolphin	5.20	0.0107	0.04	16.50	0.25	0.00
Meso Dolphin	4.81	0.0518	0.04	16.50	0.22	0.00
Sea Turtles	3.74	0.0008	0.15	3.50	0.50	0.04
Large Yellowfin	4.88	0.0198	2.35	15.60	0.36	0.15
Large Bigeye - D	5.08	0.0274	1.20	15.03	0.21	0.08
Large Marlins	5.35	0.0017	1.00	7.80	0.50	0.13
Large Sailfish	5.07	0.0002	1.15	7.80	0.25	0.15
Large Swordfish	4.86	0.0001	0.44	7.80	0.75	0.06
Large Dorado	4.82	0.0003	0.80	15.60	0.90	0.05
Large Wahoo	5.10	0.0034	1.20	9.76	0.07	0.12
Large Sharks	5.26	0.0012	0.32	7.81	0.48	0.04
Rays	4.28	0.0012	0.25	3.91	0.68	0.06
Skipjack	4.73	0.0299	1.88	21.50	0.90	0.09
Albacore	4.80	0.0093	0.77	16.95	0.75	0.05
Auxis	4.71	0.1406	2.80	8.00	0.88	0.35
Bluefin	4.67	0.0046	0.85	12.80	0.86	0.07

Group name	Trophic level	Biomass (t/km^2)	P/B (/year)	C/B (/year)	EE	P/C (/year)
Small Yellowfin	4.76	0.0250	1.75	18.30	0.86	0.10
Small Bigeye	4.63	0.0274	0.70	12.70	0.80	0.06
Small Marlins	5.37	0.0005	0.50	9.00	0.75	0.06
Small Sailfish	4.80	0.0005	0.57	9.76	0.75	0.06
Small Swordfish	4.54	0.0004	0.21	9.00	0.75	0.02
Small Dorado	4.70	0.0061	3.15	17.40	0.61	0.18
Small Wahoo	4.74	0.0081	1.75	11.40	0.78	0.15
Small Sharks	5.19	0.0032	0.58	9.16	0.84	0.06
Misc. Pisc	4.47	0.1719	2.25	7.73	0.95	0.29
Flying fish	3.45	0.2545	2.25	7.70	0.95	0.29
Misc Epi Fish	3.35	2.2491	2.07	10.78	0.95	0.19
Meso fish non-migrate (*)	3.62	1.4122	2.00	11.00	0.68	0.18
Meso fish epi migrate (*)	3.53	2.9488	2.00	10.78	0.69	0.19
Meso fish deep migrate (*) D	3.67	0.4500	2.00	6.80	0.34	0.29
Bathypelagic fish (*) D	4.48	0.0203	2.80	6.60	0.85	0.42
Cephalopods epi	4.43	0.8632	4.00	10.00	0.74	0.40
Cephalopods meso (*)	4.60	0.2368	3.50	8.50	0.93	0.41
Crabs	3.43	0.5721	3.50	10.00	0.91	0.35
Zooplankton epi (*)	2.77	1.8000	64.00	200.00	0.49	0.32
Zooplankton meso (*)	2.96	0.1199	50.00	140.00	0.90	0.36
Zooplankton deep (*) D	3.01	0.0079	45.00	110.00	0.85	0.41
Microzooplankton S ^	2.03	2.4466	143.00	600.00	0.90	0.24
Microzoo meso (*) M ^	2.28	3.3815	58.00	200.00	0.86	0.29
Microzoo deep (*) D ^	2.27	2.2305	37.00	150.00	0.86	0.25
Large Phytoplankton - S ^	1.00	1.9863	149.00		0.95	
Small Producers - S ^	1.00	6.6683	187.00		0.99	
Detritus - S ^	1.00	1.0000			0.02	
Detritus meso (*) M^	1.00	0.4000			0.64	
Detritus deep (*) D^	1.00	0.2000			0.88	

^Toxicokinetic parameters of these functional groups were modified for depth-based scenarios.

2.2 Ecotracer – modelling potential for metal bioaccumulation

Ecotracer is the routine within the EwE platform that is used to simulate the accumulation of contaminants or tracers that flow between the environment and food-web components, while biomass dynamics continue in parallel (Walters and Christensen 2018). In Ecotracer, contaminants enter biomass pools through direct uptake from the environment, food, and immigration. All producers (detritus, phytoplankton, and small producers) obtain metals from the seawater via passive absorption; hence their contaminant concentrations are controlled by their direct absorption rate. Contaminants exit the ecosystem through three primary pathways: physical or metabolic decay, biomass extraction (such as fishing mortality), and emigration of contaminated organisms. Within the ecosystem, contaminants can be transferred between ecological and environmental compartments through biological processes, including excretion by living organisms, predation events that move contaminants up food webs, decomposition of organic matter into detritus, and non-fishing mortality that releases contaminants back into the environment. The contaminant concentration over time in each functional group is based on the flow rates calculated from Ecosim, as well as decay, elimination, and physical exchange rates. The linear dynamical equation for time changes in contaminant concentration (C*i,*B*i*/dt) in each functional group *i* is represented as follows:

$$\mathrm{C}i\mathrm{B}i/\mathrm{dt} = (Cj \bullet \mathrm{GC}i \bullet Qji/Bj) + (\mathrm{u}i \bullet Bi \bullet Co) + (ci \bullet Ii) - [(\mathrm{C}i \bullet \mathrm{Q}ij/\mathrm{B}i) \\ + \mathrm{C}i \bullet MOi + ((1 - \mathrm{GC}i) \bullet \sum jCj \bullet Qji/Bj + ei \bullet Ci + di \bullet Ci) \quad (1)$$

The description of the equation terms is as follows:

Uptake from food: *Cj* • *GCi* • *Qji/Bj* where *Cj* = contaminant concentration in food j, *GCi* = proportion of food assimilated by type *i* organisms; *Qji* = biomass flow rate from *j* to *i* (estimated in Ecopath as *Bi* • (*Q/B*)*I* • *DCij*), *Bj* = food j biomass;

Direct uptake from environment: *ui* • *Bi* • *Co*, where *ui* = parameter representing uptake per biomass per time, per unit environmental concentration, *Bi* = biomass, *Co* = environmental concentration;

Concentration in immigrating organisms: *ci* • *Ii*, where *ci* = parameter (tracer per unit biomass in immigrating biomass), *Ii* = biomass of pool *i* immigrants per time;

Predation: *Ci* • *Qij/Bi*, where *Ci* = concentration in pool *i*, *Qij* = consumption rate of type *i* organisms by predator type j, *Bi* = biomass in pool *i*;

Detritus: *Ci* • *MOi* + (1 − *GCi*) • *∑jCj* • *Qji*/*Bj*, where *MOi* = non-predation death rate of type *i* (per year), *GCi* = fraction of food intake assimilated, *Qji* = intake rate if type *j* biomass by type *i*;

Emigration: *ei* • *Ci*, where *ei* = emigration rate (per year);

Metabolism: *di* • *Ci*, where *di* = metabolism + decay rate for the material while in pool *i*.

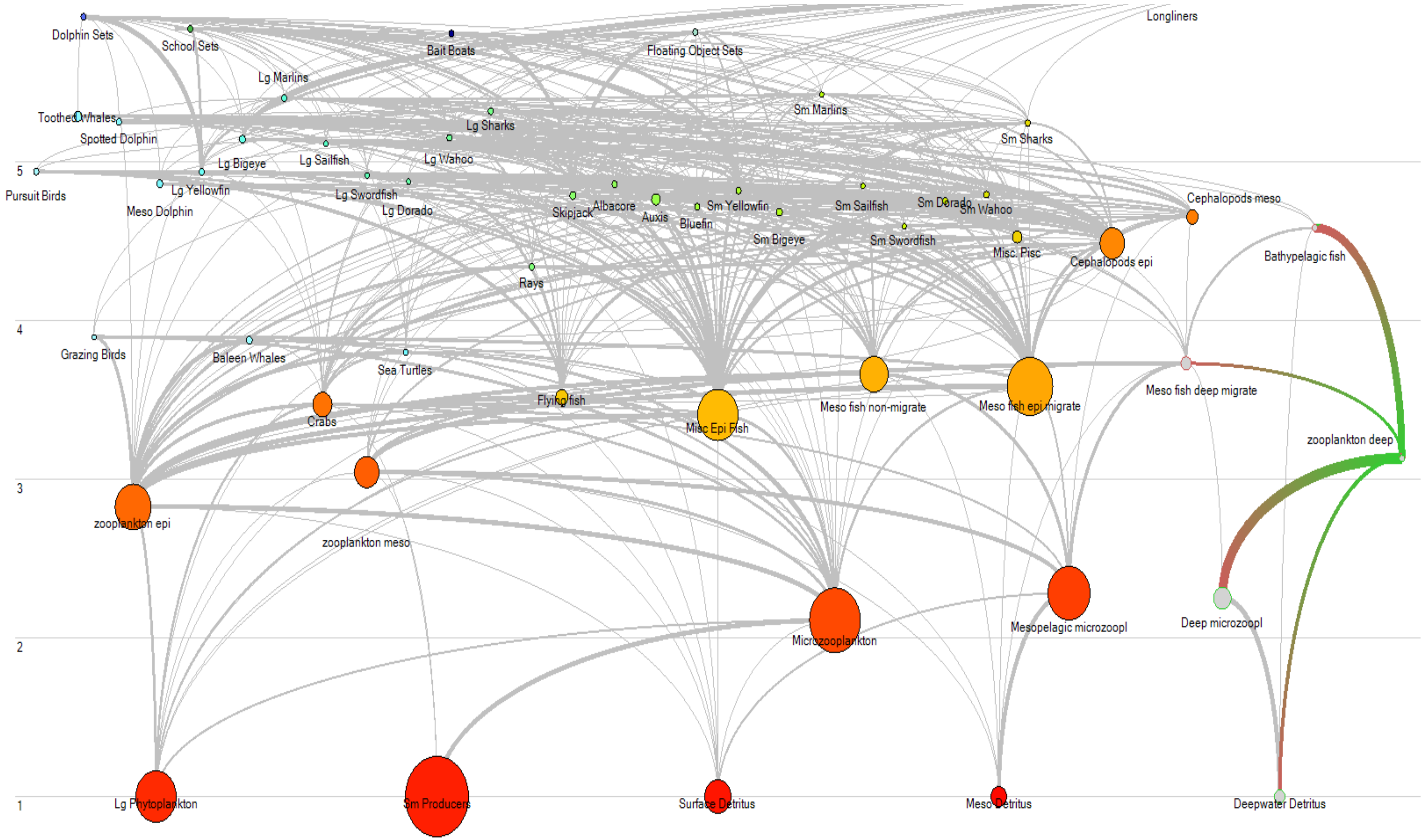

Figure 1. Food web structure of the updated EwE ETP model primarily used in this study to evaluate the risk of metal bioaccumulation in epipelagic, mesopelagic and bathypelagic ocean biota. Bathypelagic (1,000 – 3,000 m) food web connections are highlighted with width of the line indicating the degree of energy exchange via deep zooplankton.

2.3 Metal concentrations

Metals concentration data were obtained from the Texas A&M University (TAMU) who characterized the chemical composition of the water column of the NORI-D lease within the CCZ and measured within near-field (<200 m) and far-field (>200 m) midwater discharge plumes, which were released in the pilot mining trials at ~1,250 m (Fitzsimmons *et al.* 2025). The Collector Test Report measured a large array of analytes present in the water column and in plume discharges which were categorised into: biologically-active elements, potentially hazardous chemicals, and particles. Our study was focused on tracing potentially hazardous chemicals along with other essential metals which were categorised by toxicity, bioaccumulative potential, and persistence:

1. Metal Group 1. Highly toxic, bioaccumulating and persistent potentially hazardous metals including lead (Pb), cadmium (Cd) and mercury (Hg).
2. Metal Group 2. Moderately toxic and persistent potentially hazardous metals including copper (Cu), zinc (Zn), nickel (Ni), and manganese (Mn).
3. Metal Group 3. Essential and non-toxic biologically-active elements including iron (Fe) and labile cobalt (Co).

Decay rates (/year) in the environment were set at zero for Metal group 1; 0.08 for Metal group 2; and 0.2 for Metal group 3 to reflect literature on residence times in oceanic waters (Bruland and Lohan 2004; Sohrin and Bruland 2011, Balistrieri *et al.* 1981).

Background metal concentrations, required to calculate the initial environment conditions (t/km^2) for the Ecotracer model, were based on data provided by TAMU (Table 2-3). These background measurements were collected by TAMU following GEOTRACES protocols for trace metal sampling and analysis. Data were obtained from the NORI-D Collector Test using water samples conducted prior to any plume discharge at ~1,200 m depth during 2021–2022 (Fitzsimmons *et al*. 2025). The reported metal concentrations were in dissolved form for most elements which are considered more bioavailable as these species can be directly assimilated by organisms through diffusion, ingestion, or membrane transport mechanisms. Total mercury and methylmercury were also reported. For each metal group, we calculated the mean concentration of all measured elements assigned to that group. To convert these values into Ecotracer modelled environment we assumed an average depth of 4,000 m and applied the surface area of the model domain (32,800,000 km^2).

For the baseline simulations, we used a background concentration of 0.0000307 t/km^2 for Metal group 1, 0.015 t/km^2 for Metal group 2, and 0.3 t/km^2 for Metal group 3. Most metals background concentrations fell within the acceptable ranges of published studies (Morell and Price 2003; Hatje *et al.* 2018; Sohrin and Bruland 2011) and the global GeoRem database (Jochum *et al.* 2005). For Metal group 1, our background concentration falls within the range of those reported across the Pacific Ocean (0.08–0.52 ng/L; Bowman *et al.* 2016; Chen and Li 2019; Starr *et al.* 2025). For Metal groups 2 and 3 our background concentrations fell within the ranges reported for Nickel (300–2,000ng/L), Zn (60–800ng/L), Mn (20–400ng/L), Cu (30–200ng/L), Co (10–60ng/L) and dissolved iron (1–80ng/L) (Moore and Braucher 2007; Bruland and Lohan 2004; Fitzsimmons *et al.* 2016).

Baseline simulations incorporated fixed inflow rates to represent annual metal inputs from atmospheric deposition and volcanic sources. For Metal group 1, an inflow rate of 0.0000021 t/km^2/year was used to maintain a constant background concentration. This inflow rate was lower than that estimated by von Helfeld *et al.* (2023), 0.000024 t/km^2/year based on a global annual input of 8800 t/year. Nevertheless, our estimate aligns with reported global atmospheric input to the ocean which range from 1.1 to 1.9 Gg of THg per year (Streets *et al.* 2011, Muntean *et al.* 2014; Zhang *et al.*2023). For Metal group 2, we used a baseline inflow rate of 0.003 t/km^2/year based on global input estimates of 360 million moles Ni per year (Sweer *et al.* 2023). For Metal group 3 we calculated inflow rate on Fe at 0.0091 t/km^2/year based on the upper global ocean range of between 0.2–0.4 Tg labile iron atmospheric deposition per year (Moore and Braucher 2007; Myriokefalitakis *et al.* 2019).

Table 2-3. Metal concentrations (ng/L) of the background environment at ~1,200 m (baseline and pre-mining) and directly within midwater discharge plumes as measured by Texas A&M University (Fitzsimmons *et al.* 2025).

	Background (ng/L)		Midwater plume (ng/L)^	
	minimum	**maximin**	**minimum**	**maximum**
Metal group 1: highly toxic, post-transition metals				
Total mercury (Hg)	0.09	0.42	0.10	0.40
Methylmercury (MeHg)	0.00	0.22	0.01	0.22
Dissolved lead (dPb)	0.00	6.37	0.00	65.84
Dissolved cadmium (dCd)	0.00	115.22	106.00	131.35
Metal group 2: moderately toxic, heavy transition metals				
Dissolved zinc (dZn)	8.04	671.49	424.20	853.50
Dissolved nickel (dNi)	141.38	585.96	363.97	2020.79
Dissolved manganese (dMn)	6.19	115.44	7.32	31087.86
Dissolved copper (dCu)	51.46	346.52	99.66	909.93
Metal group 3: essential, non-toxic				
Dissolved iron (dFe)	6.87	41.79	12.59	49170.00
Labile cobalt (pCo)	0.00	4.83	1.21	160.08

^Concentrations were measured within near-field (<200 m) and far-field (>200 m) midwater discharge plumes, which were released in the pilot mining trials at ~1,250 m depth. These concentrations do not consider plume dilution through mixing back into the ocean at the discharge depth.

Concentrations of metals at the time of plume discharge, needed to calculate inflow rates (g/*km*^{2}/year) for the model exposure scenarios, were provided by TAMU (Table 2-3). These measurements were taken from trace metal water sampling directly from within the discharge plume released in the pilot mining trials at ~1,250 m (Fitzsimmons *et al.* 2025). To convert concentration data to exposure inflow rates (t/*km*^{2}/year) we used standard mass and time conversions, a discharge rate of 0.5 m^3/s and a plume area of 6 *km*^{2}. When scaled to the full model domain, the exposure inflow rates translate to extremely low concentrations. For example, even high local concentrations of Metal group 1 result in an average of 4.19×10^{-12} t/*km*^{2}/year when evenly distributed across the entire area; well below baseline inflow rates based on natural inputs. To explore potential impacts, we thus tested +5%, +10%, +20% and +50% increases above baseline inflow rates. These tests did not individually account for the fact that discharge occurs in a restricted and much smaller area than the overall model domain. Instead, the simulations explored potential impacts of supplementary inputs exceeding natural baseline levels, accounting for exchange processes in and out of the plume area and the potential persistence of contaminants within the plume. Finally, we also ran a reference baseline simulation where there was no release of plume associated metals (*i.e.,* baseline values were held at the original values stated above).

To estimate initial concentrations and uptake parameters for the functional groups we used values, where available, from published literature. For Metal group 1 (highly toxic and persistent metals), we adopted initial concentrations and elimination rates (yr^{-1}) from the original ETP EwE model developed for tracing mercury (Ferriss and Essington 2014). For taxa groups that didn't have such information we based concentrations on similar physiological taxa groups. For example, the same initial concentration was used for all mesopelagic fish functional groups (shallow and deep migrators and non-migrators). For Metal groups 2 and 3, we commenced with zero concentrations and ran the model for 20 years under background environment concentrations, before then re-running the model with these new initial concentrations (Table 4).

For Metal group 1, initial concentrations spanned from a minimum of 0.043 $\mu g\ g^{-1}$ in miscellaneous epipelagic fish to a maximum of 4.12 $\mu g\ g^{-1}$ in large sharks. For Metal group 2, the lowest concentration in consumers was 0.03 $\mu g\ g^{-1}$ in crabs, while the highest was 44.37 $\mu g\ g^{-1}$ in large wahoo. For Metal group 3, initial concentrations in consumers ranged from a 15.54 $\mu g\ g^{-1}$ in *Auxis* (a small tuna-like species) to a maximum of 503.42 $\mu g\ g^{-1}$ in large bigeye tuna. For all Metal groups, concentrations initially declined before stabilising around 10 years. This initial phase was treated as a simulated 'burn-in' period and then followed by model scenarios extending for a further 20-years.

To represent differences in transport and availability between the three metal groups, we altered some additional Ecotracer input parameters (App. Table 2). For Metal group 1 we applied an assimilation efficiency rate of 85% for all mid and higher levels consumers, while plankton were 100% efficient. For Metal groups 2 and 3 we used assimilation efficiencies of 70% and 50% for consumers, and 80% and 60% for plankton, based on their reduced bioavailability, potential for rapid excretion, and weaker binding affinity in biological tissues. These values are comparative to those used in previous modelling studies (Ferriss and Essington 2014; Li *et al.* 2022) and are supported by experimental evidence and comparative studies indicating species- and metal-specific differences in assimilation, particularly for essential versus non-essential metals and those with differing chemical speciation and lability in the marine environment (Mathews *et al.* 2008; Xu *et al.* 2001; Wang *et al.* 2002). For all metal groups we applied zero concentrations in immigrating biomass for all functional groups and imposed direct uptake rates (g/g/day) on phytoplankton (0.1), microzooplankton (0.05) and zooplankton (0.01). These values are at the upper end of uptake rates reported in previous contaminant modelling studies (*e.g.,* Arnot and Gobas 2004; De Laender *et al.* 2015), and were selected to represent plausible metal accumulation dynamics under varying exposure scenarios.

We ran a simple linear regression of modelled metal concentrations across the entire food web against their respective trophic levels as previously determined by Hoover *et al.* (2021). The

Trophic Magnification Factors (TMF) was calculated for each metal group as the antilog of the regression slope:

$$\text{TMF} = 10^{b}$$

where *b* is the slope of the linear regression between the log10 transformed metal concentrations.

2.4 Sensitivity analyses

To investigate the most influential parameters responsible for metal bioaccumulation in the food web (as represented in our model), we conduct sensitivity analyses of seawater and producer metal concentrations and the Ecotracer parameters related to metal uptake, biotransformation, and elimination in each broad biota category (*i.e.,* producers, zooplankton, fish, and marine mammals). We perturbed each parameter by ±10% of the original amount, and the sensitivity was calculated as:

$$Sensitivity = \frac{\triangle \mathrm{y}/\mathrm{y}}{\triangle x/x}$$

where *x* is a specific parameter and *y* is the simulated metal concentration of each organism. $\triangle y$ is the change in the metal concentration (*y*) because of the change ($\triangle$x) of the input parameter. $\triangle x/x$ is fixed as 10% in our sensitivity analysis.

2.5 Scenarios

We ran several between and within-model simulations to explore the effects of discharging metal concentrations into oceanic ecosystems (Table 2-4). The updated ETP models was used to explore the effects of low and high concentrations of different metal groups and assess the risk of bioaccumulation to increase concentrations over the whole ecosystem and then at two different depths or vertical zones including the mesopelagic zone (200–1,000 m) and the deep bathypelagic zone (1,000–3,000 m). Inflow rates were increased by 5% and 10% above baseline values to simulate potential additional metal inputs from plume discharges. These moderate increases were applied across all metal groups and scenario runs to assess the sensitivity of food web responses to elevated exposure. To explore upper-bound ecological responses under highly localised and extreme conditions, inflow rates were also increased by 20% and 50% above baseline values, representing severe, localised contaminant enrichment scenarios.

To approximate depth-specific exposure in a non-spatial Ecotracer model, we set direct absorption rates to zero and imposed high decay rates on selected (non-impacted) functional groups. This method allowed us to simulate depth-restricted exposure scenarios (*e.g.*, bathypelagic vs. mesopelagic zone discharge events) by functionally isolating unaffected trophic groups. For the bathypelagic discharge scenario (1,000–3,000 m), a direct absorption rate of zero was given to all epipelagic and mesopelagic producers and first-order consumers, including phytoplankton, small producers, pelagic microzooplankton, and mesopelagic microzooplankton. In contrast, for discharges in mesopelagic zone (200–1,000 m), the same parameter adjustments were applied to epipelagic producers and the deep microzooplankton groups, limiting their exposure while allowing all other functional groups to interact with the discharged metals. Because detritus can act as a pathway for contaminant transfer, we applied very high decay rates to habitat zones not directly affected by the discharge depth. This was considered an indirect way to simulate vertical structure in a non-spatial Ecotracer model, which does not allow for varying inflow concentrations by functional group. While this approach introduces simplifications, it enabled an initial exploration of depth-specific metal exposure effects within the constraints of the current model configuration.

Table 2-4. Summary of model scenarios examined in this study. Gray boxes denote unsimulated scenarios.

Scenario		Plume Depth			Additional models	
		Whole ecosystem	**Mesopelagic (200–1,000 m)**	**Bathypelagic (1,000–3,000 m)**	**WTPO**	**NCC**
Metal group 1. Highly toxic, bioaccumulative, persistent (Hg, Pb, Cd)	*Baseline*	W_M1	M_M1	D_M1	WTPO_M1	NCC_M1
	+5%	W_M1_10	M_M1_10	D_M1_10	W_M1_20	N_M1_250
	+10%	W_M1_20	M_M1_20	D_M1_20	W_M1_50	N_M1_50
	+20%	W_M1_L	M_M1_L	D_M1_L	W_M1_L	N_M1_L
	+50%	W_M1_H	M_M1_H	D_M1_H	W_M1_H	N_M1_H
Metal group 2. Moderately toxic, bioaccumulative, persistent (Cu, Zn, Ni, Mn)	*Baseline*	W_M2				
	+5%	W_M2_20				
	+10%	W_M2_50				
	+20%	W_M2_L				
	+50%	W_M2_H				
Metal group 3. Low toxicity, reduced persistent and low BAF (Fe, Al, Co)	*Baseline*	W_M3				
	+5%	W_M3_20				
	+10%	W_M3_50				
	+20%	W_M3_L				
	+50%	W_M3_H				

To address uncertainty in trophic structure and biomass flows, we applied the baseline toxicokinetic parameters for metal group 1 to a second previously published EwE models (WTPO). This approach enabled us to evaluate whether comparable bioaccumulation risks were evident in other oceanic ecosystems similar to that performed by Ferris and Essington (2014).

Ecotracer outputs are presented as changes in concentration per unit $\mu g\ g^{-1}$ and as percentage relative differences (%) from the baseline scenario. All models had a 10-year burn in before then being run over a 20-year period, with 5-year averages calculated to reduce model noise and highlight short to longer-term trends.

2.6 Threshold based bioaccumulation classification

To assess the severity of bioaccumulation of metal group 1 (*e.g.,* lead, cadmium, and mercury) in the two modelled ecosystems (mesopelagic and bathypelagic), we applied a four-tiered bioaccumulation classification framework. This approach categorises the magnitude of simulated concentration increases ($\mu g\ g^{-1}$) from mid-water discharge plumes relative to internationally recognised seafood safety thresholds for each metal group (Table 2-5 and App. Table 1).

Importantly, the framework considers cumulative exposure, incorporating additional metal loadings from potential mid-water discharges on top of background bioaccumulation arising from baseline natural and anthropogenic sources already operating in the system. The classification is intended to support interpretation of model outputs across different exposure intensities. While we propose a graded classification scheme to aid assessment, we acknowledge that final decisions on threshold definitions remain the responsibility of the International Seabed Authority (ISA). The classification thresholds used in this study are defined as follows:

1. **Non-detectable**: No measurable increase in concentration, including very small changes (zero to 1.0E-07 μg g^{-1}) considered negligible and below the detection limits of standard analytical instruments.
2. **Low**: A minimal increase, between zero and 1% of the health advisory threshold.
3. **Medium**: Increases between 1% and 10% of the health advisory threshold.
4. **High**: Increases greater than 10% of the health advisory threshold.

The framework provides a scalable way to compare potential impact across different functional groups.

Table 2-5. Concentration ranges (*μg g^{-1}*) for each metal group, classified in reference to health advisory thresholds (as concentrations that cause harmful effects) established by international guideline authorities (App. Table 1).

	Non-detectable	Low	Medium	High	Advisory threshold
metal group 1	0 – 1.0E-07	1.0E-07 – 0.003	0.003 – 0.03	>0.03	0.3 μg g^{-1}
metal group 2	0 – 1.0E-07	1.0E-07 – 0.03	0.03 – 0.3	>3.0	30 μg g^{-1}
metal group 3	0 – 1.0E-07	01.0E-07 – 0.5	0.5 – 5.0	>5.0	50 μg g^{-1}

3 Results

3.1 Updated Ecopath with Ecosim model outputs

The 49 functional groups were organised into approximately five trophic levels, with large marlin and sharks occupying the top of the ETP food web (Figure 1). Within the final balanced Ecopath model, the five primary producer groups accounted for 34% of the total system biomass, while apex predator groups (trophic level >4.5) accounted for 2.3%. Zooplankton accounted for 0.4% in the mesopelagic zone and 0.03% in the deep ocean. Trajectories of relative biomass for most functional groups stabilised after 10 years (Figure 2). This burn-in change in biomasses reflects the influence of implicit vertical spatial structure on the time varying stable biomasses versus the Ecopath defined initial conditions. Given the relative uncertainty in the biomasses of these deeper groups, even a three-fold difference is within plausible biomass bounds for these groups. Consequently, the model is considered scenario-ready if all treatments are run post the initial 10-year burn-in.

Predator consumption rates responded to changes in vulnerability values as expected, decreasing with lower vulnerability and increasing with higher values.

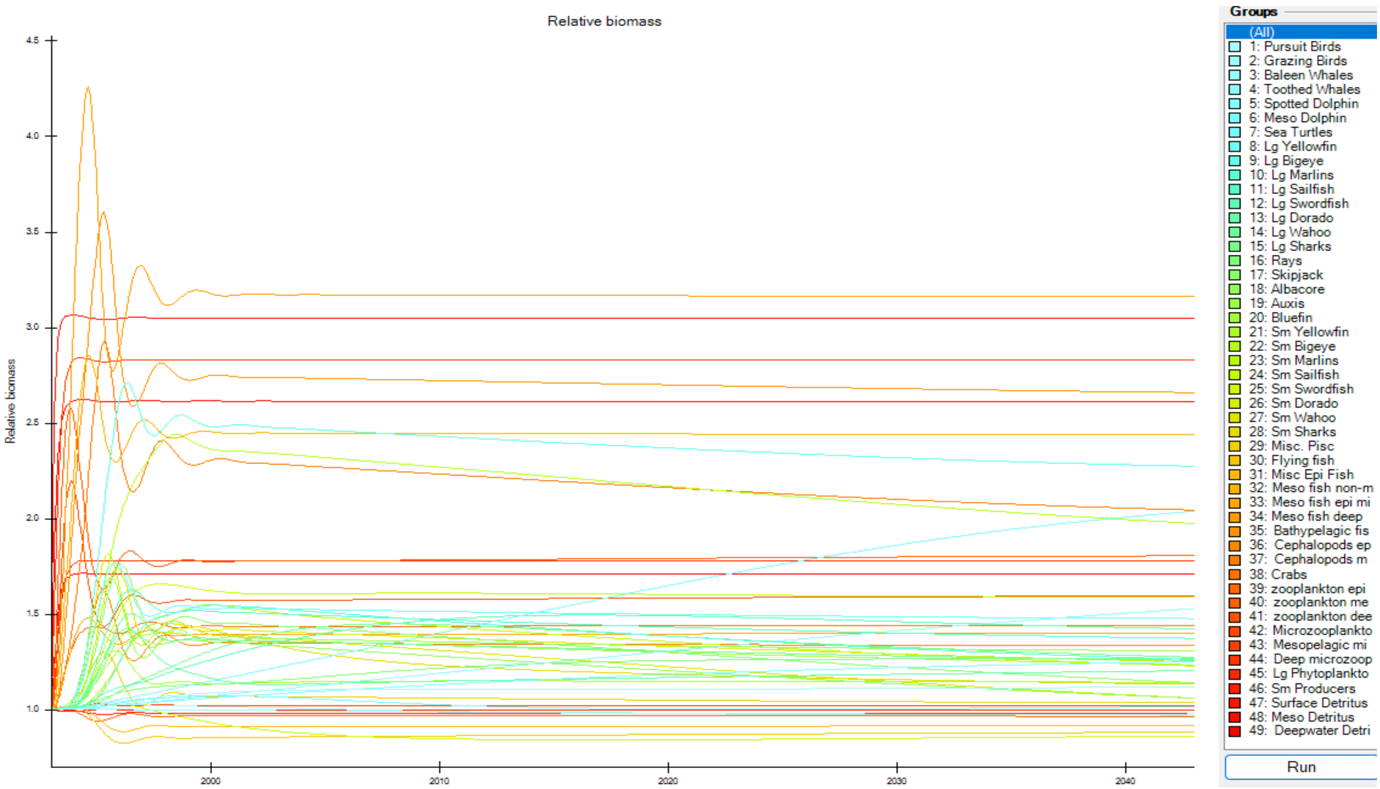

Figure 2. Ecosim simulation demonstrating steady states of relative biomass for most functional groups after 10 years. In model scenario runs, the first 10 years were removed and classified as the model burn-in period.

3.2 Scenario outputs

3.2.1 Metal group baselines and bioaccumulation differences (whole ecosystem)

Model outputs for different metal groups show substantial variation in metal concentrations across marine functional groups, with distinct patterns emerging by trophic position. Simulated concentrations were highest for Metal group 3, followed by Metal group 2 and Metal group 1, consistent with their respective background and baseline inflow levels in the environment (Table 2-3).

Concentrations of metal group one, under baseline (constant, natural source influxes) conditions for the whole ecosystem at year 5, ranged between 0.003 and 1.0 $\mu g\ g^{-1}$ in high order consumers with the lowest levels in crabs and flying fish and largest concentrations in large and small sharks and swordfish. After 15 years of simulations, only large sharks and marlin had simulated concentrations above the threshold levels of 0.3 $\mu g\ g^{-1}$ (App. Figure 1). Concentrations in large phytoplankton reached 0.00025 $\mu g\ g^{-1}$, microzooplankton 0.00105 $\mu g\ g^{-1}$ and zooplankton between 0.002110 and 0.00235 $\mu g\ g^{-1}$.

After five years of simulated discharge, metal group 1 showed minimal change under both +20% and +50% inflow scenarios, with increases of less than 1.2% across all functional groups (Table 3-1). Under the +50% scenario, metal group 2 increased by 0.1–19%, while Metal group 3 exhibited relative increases ranging from 0.3% to 44.3%. For all metal groups, largest relative increases were observed in lower and mid-trophic groups while smaller relative increases were observed in rays, large sharks, marlin, sailfish, and swordfish.

Table 3-1. Simulated concentrations (C, µg/g) and relative differences (%) in concentrations for the three metal groups and each functional group in order of decreasing trophic position after 10 years under +20% and +50% exposure scenarios compared to the food web model under baseline inflow rates. These results represent the whole ecosystem and assume uniform dispersion of the discharge plume throughout the water column of the entire model domain (0–3,000 m).

	Metal group 1 (highly toxic)			Metal group 2 (mod. toxic)			Metal group 3 (non-toxic)		
Group name	C	+20%	+50%	C	+20%	+50%	C	+20%	+50%
Small Marlins	0.411	0.1	0.2	7.27	0.3	0.8	87.46	6.4	15.8
Large Marlins	0.196	0.2	0.4	3.50	1.2	3.0	42.24	6.2	15.4
Large Sharks	1.001	0.0	0.1	11.39	0.2	0.5	194.29	2.8	7.1
Toothed Whales	0.069	0.5	0.9	0.92	6.2	15.5	7.36	17.3	43.1
Spotted Dolphin	0.109	0.5	1.0	1.91	6.5	16.3	13.19	17.5	43.4
Small Sharks	0.293	0.2	0.3	5.40	1.1	2.7	82.25	4.8	12.0
Large Wahoo	0.069	0.5	1.0	1.48	6.3	15.8	16.90	17.3	43.0
Large Bigeye	0.053	0.5	1.0	1.33	6.5	16.3	17.38	17.3	43.1
Large Sailfish	0.051	0.2	0.4	0.99	0.9	2.3	14.70	5.2	12.9
Large Yellowfin	0.021	0.6	1.1	0.50	7.0	17.5	5.94	17.6	43.7
Pursuit Birds	0.011	0.6	1.1	0.38	7.2	17.9	1.56	17.7	43.9
Large Swordfish	0.225	0.0	0.0	3.18	0.1	0.2	33.18	14.2	35.3
Large Dorado	0.070	0.4	0.8	1.81	5.3	13.4	23.59	17.3	43.0
Meso Dolphin	0.079	0.5	1.0	1.27	6.6	16.6	12.01	17.5	43.5
Albacore	0.055	0.5	1.1	1.25	6.7	16.8	13.26	17.5	43.5
Small Sailfish	0.064	0.4	0.7	1.51	3.8	9.4	19.26	17.2	42.8
Small Yellowfin	0.032	0.5	1.1	0.80	6.9	17.3	9.24	17.6	43.7
Small Wahoo	0.025	0.5	1.1	0.72	6.8	17.0	10.41	17.5	43.5

	Metal group 1 (highly toxic)			Metal group 2 (mod. toxic)			Metal group 3 (non-toxic)		
Group name	C	+20%	+50%	C	+20%	+50%	C	+20%	+50%
Skipjack	0.042	0.5	1.1	1.14	6.9	17.2	14.62	17.5	43.6
Auxis	0.005	0.6	1.1	0.10	7.2	17.9	1.03	17.7	43.9
Small Dorado	0.020	0.6	1.1	0.61	7.0	17.5	9.35	17.6	43.7
Bluefin	0.030	0.5	0.9	0.81	6.0	15.1	12.63	17.2	42.7
Small Bigeye	0.059	0.5	1.0	1.73	6.1	15.2	20.16	17.1	42.6
Cephalopods meso	0.007	0.6	1.1	0.18	7.1	17.9	2.52	17.6	43.9
Small Swordfish	0.646	0.0	0.0	5.34	0.0	0.1	36.87	0.1	0.3
Bathypelagic fish	0.008	0.6	1.1	0.11	7.3	18.1	3.91	17.6	43.7
Misc. Piscivores	0.005	0.6	1.1	0.10	7.2	17.9	1.20	17.6	43.9
Cephalopods epi	0.007	0.6	1.1	0.29	7.1	17.7	3.24	17.6	43.9
Rays	0.363	0.0	0.0	1.59	0.1	0.3	107.21	1.1	2.7
Grazing Birds	0.005	0.6	1.2	0.12	7.4	18.6	1.65	17.7	44.1
Baleen Whales	0.026	0.5	1.0	0.72	6.8	16.9	11.43	17.5	43.6
Sea Turtles	0.015	0.2	0.4	0.43	2.5	6.3	6.95	17.3	43.1
Meso fish deep migrate	0.003	0.6	1.2	0.10	7.3	18.4	1.74	17.7	44.0
Meso fish non-migrate	0.004	0.6	1.2	0.15	7.4	18.4	2.88	17.7	44.1
Meso fish epi migrate	0.004	0.6	1.2	0.16	7.4	18.4	3.29	17.7	44.1
Flying fish	0.003	0.6	1.2	0.16	7.3	18.3	3.73	17.7	44.0
Crabs	0.003	0.6	1.2	0.14	7.3	18.2	3.49	17.7	44.0
Misc Epi Fish	0.005	0.6	1.2	0.22	7.3	18.2	5.01	17.7	44.0
Zooplankton deep	0.003	0.6	1.2	0.17	7.5	18.8	4.24	17.8	44.2
Zooplankton meso	0.002	0.6	1.2	0.13	7.5	18.9	3.70	17.8	44.2
Zooplankton epi	0.002	0.6	1.2	0.14	7.6	18.9	4.69	17.8	44.2
Meso microzoopl	0.0001	0.6	1.2	0.06	7.5	18.9	1.74	17.8	44.2
Deep microzoopl	0.0002	0.6	1.2	0.10	7.5	18.8	2.96	17.8	44.2
Microzooplankton	0.0001	0.6	1.2	0.07	7.6	18.9	2.46	17.8	44.2
Large Phytoplankton	0.00002	0.6	1.2	0.02	7.6	19.0	0.84	17.8	44.2
Sm Producers	0.00002	0.6	1.2	0.02	7.6	19.0	0.66	17.8	44.3
Surface Detritus	0.00002	0.6	1.2	0.0005	7.4	18.5	0.47	17.7	44.1
Meso Detritus	0.00002	0.6	1.2	0.0002	7.5	18.8	0.07	17.8	44.2
Deepwater Detritus	0.00002	0.6	1.2	0.0004	7.5	18.8	0.11	17.8	44.2

The calculated trophic magnification factor (TMF) for metal group 1 was 4.97, 3.38 for metal group 2 and 2.53 for metal group 3 (Figure 3). These differences agree with the simulated extents of biomagnification with higher values indicating higher biomagnification. The three outliers for Metal group 3 include large sharks, rays and small swordfish indicating higher concentrations relative to their trophic position. All models revealed a clear biomagnification trend, with minimal accumulation at lower trophic levels and disproportionate increases in large, long-lived predators.

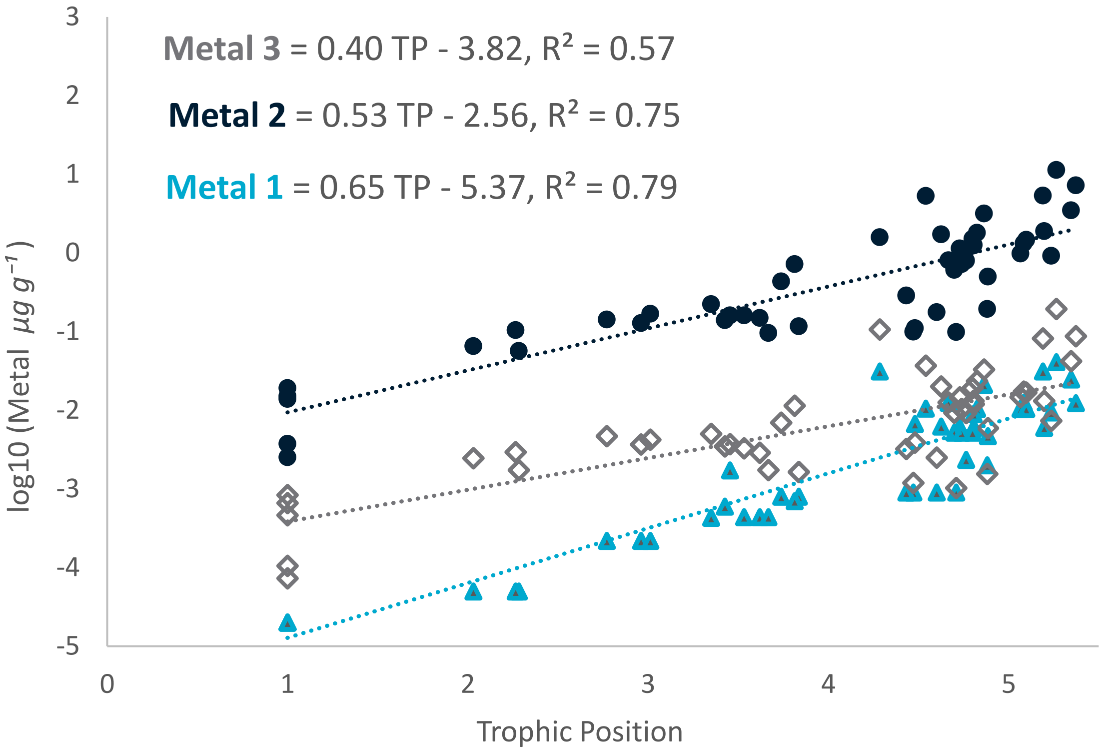

Figure 3. Relationships between the logarithm (log10) of projected contaminant concentrations (ng/g) of the three metal groups examined in this study relative to trophic position (TP). Metal group 1 – heavy, post-transition metals that bioaccumulate and are highly toxic (*e.g.*, Hg, Cd, and Pb); Metal group 2 – heavy transitional metals such as Zn, Ni, Mn and Cu; Metal group 3 – Essential elements such as Fe and Co. The apparent trophic magnification factor (TMF) was calculated from the slopes of the relationships.

3.2.2 Effects of discharge depth and inflow concentrations (metal group 1)

Metal accumulation patterns differed markedly between mesopelagic (200–1,000 m) and deep (>1,000 m) discharge scenarios, with distinct responses observed across the three vertically connected food webs (Figure 4 and Figure 5). Under the mesopelagic discharge scenarios, metal concentrations increased progressively with exposure duration in 45 functional groups (excluding primary producers and microzooplankton as they had uptake rates of zero). Mesopelagic top predators exhibited the highest levels of bioaccumulation. After 15 years of simulated +50% baseline exposure, large sharks showed the greatest relative increase above baseline (0.018 $\mu g\ g^{-1}$), followed by large marlins (0.015 $\mu g\ g^{-1}$). Small sharks, small marlin, swordfish, bigeye, spotted dolphin and toothed whales all showed increases of between 0.0025 and 0.0075 $\mu g\ g^{-1}$ under extended exposure (at 15 years simulated +50% exposure) (Figure 5).

Under the mesopelagic discharge scenarios, metal group 1 concentrations in zooplankton groups increased by 0.00018 $\mu g\ g^{-1}$ (mesopelagic) and 3.8E-05 $\mu g\ g^{-1}$ (epipelagic) under the simulated +50% baseline exposure. Concentrations in microzooplankton increased by 9.9E-05 $\mu g\ g^{-1}$ (mesopelagic) and 1.3E-05 $\mu g\ g^{-1}$ (epipelagic) under +50% baseline exposure. The mesopelagic scenario also saw increases of concentrations in the deep bathypelagic fish groups, via the detritus and mesopelagic deep migrating fish pathways, but concentrations increases were 51–53% less than those under the deep ocean discharge scenarios.

Deep discharge scenarios resulted in non-detectable (zero or <1.0E-07 $\mu g\ g^{-1}$) increases over 20 years in all epipelagic and mesopelagic top-order predator functional groups. Only bathypelagic fish showed measurable concentration increases reaching 0.0007 $\mu g\ g^{-1}$ at 15 years of simulated +50% baseline inflow rates. When small trophic connections to deep-migrating mesopelagic fish, bigeye tuna, and toothed whales were included, contaminant concentrations in all three groups increased marginally but remained below 1.0E-07 $\mu g\ g^{-1}$ after 15 years at +50% inflow. Under the bathypelagic scenarios deep zooplankton increased 0.0005 $\mu g\ g^{-1}$ (+50% baseline inflow rates) while there was zero concentration increases for mesopelagic and epipelagic zooplankton. These increases were an order of magnitude higher than those simulated for equivalent mesopelagic and epipelagic zooplankton concentrations under mesopelagic discharge scenarios. A similar pattern was observed for microzooplankton and detritus, with higher concentrations in these deep dwelling lower trophic groups occurring under the deep ocean discharge scenario.

For both the mesopelagic and the deep ocean discharge scenarios, lower trophic level functional groups including detritus, microzooplankton and larger zooplankton groups, demonstrated metal concentration increases, consistently below 0.0001 $\mu g\ g^{-1}$ under simulated +50% exposure.

The results demonstrate the potential for strong trophic magnification effects, when released into depths where prey species or sources reside, with metals preferentially accumulating in large, long-lived, highly mobile pelagic predators in those circumstances. Simulations over time also revealed consistent increases in metal concentrations, confirming the cumulative nature of bioaccumulation in apex predators.

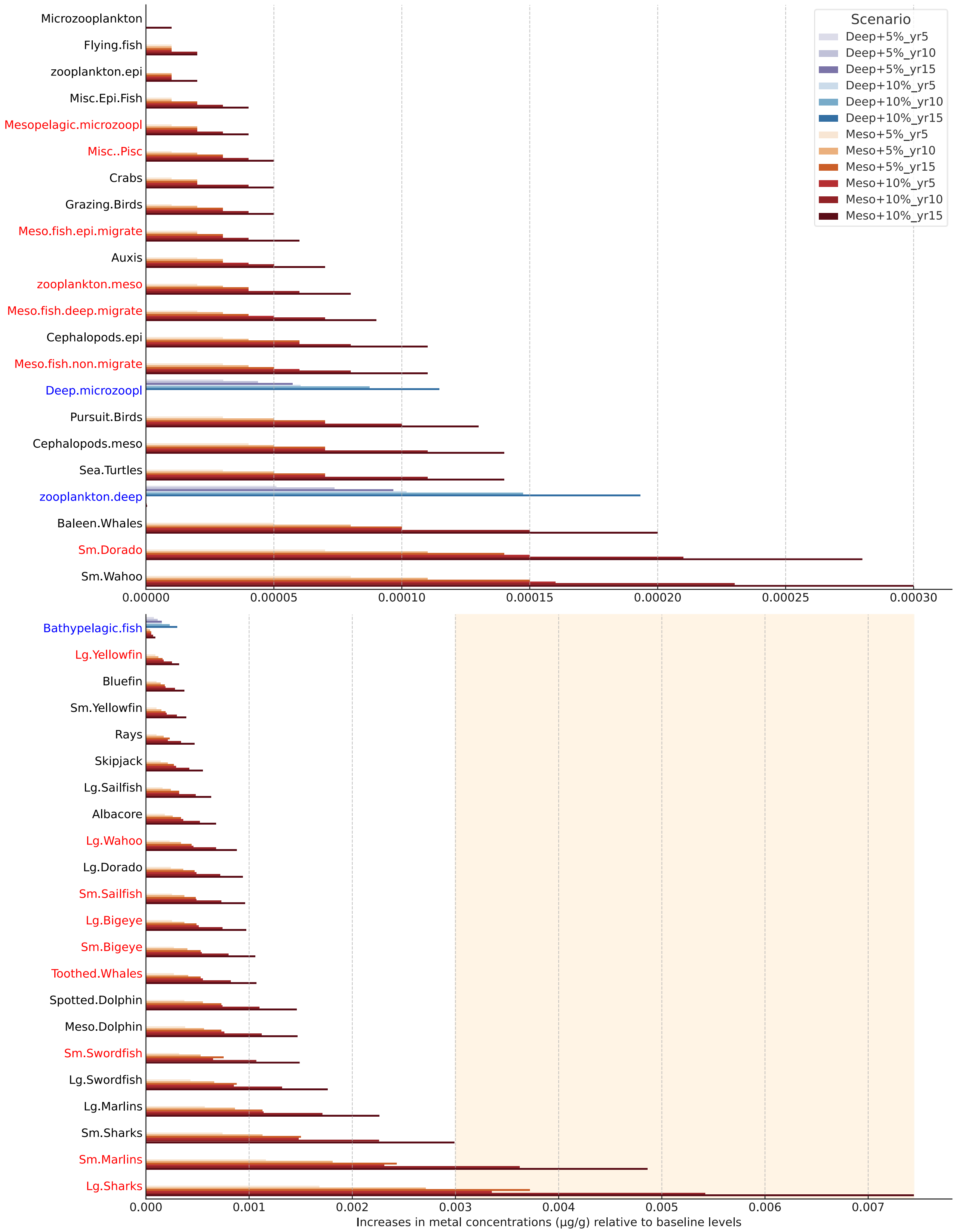

Figure 4. Relative increases in concentrations ($\mu g\ g^{-1}$) of metal group 1 after 5, 10 and 15 years across all consumer functional groups, under baseline concentrations +5% and +10% mesopelagic (200–1,000 m) and bathypelagic (1,000–3,000 m) discharge scenarios. Taxa primarily feeding in epipelagic, mesopelagic and bathypelagic habitats are noted in black, red, and blue text. Yellow shading indicates medium level concentration increases of between 1% and 10% of the health advisory threshold for metal group one of 0.3 $\mu g\ g^{-1}$.

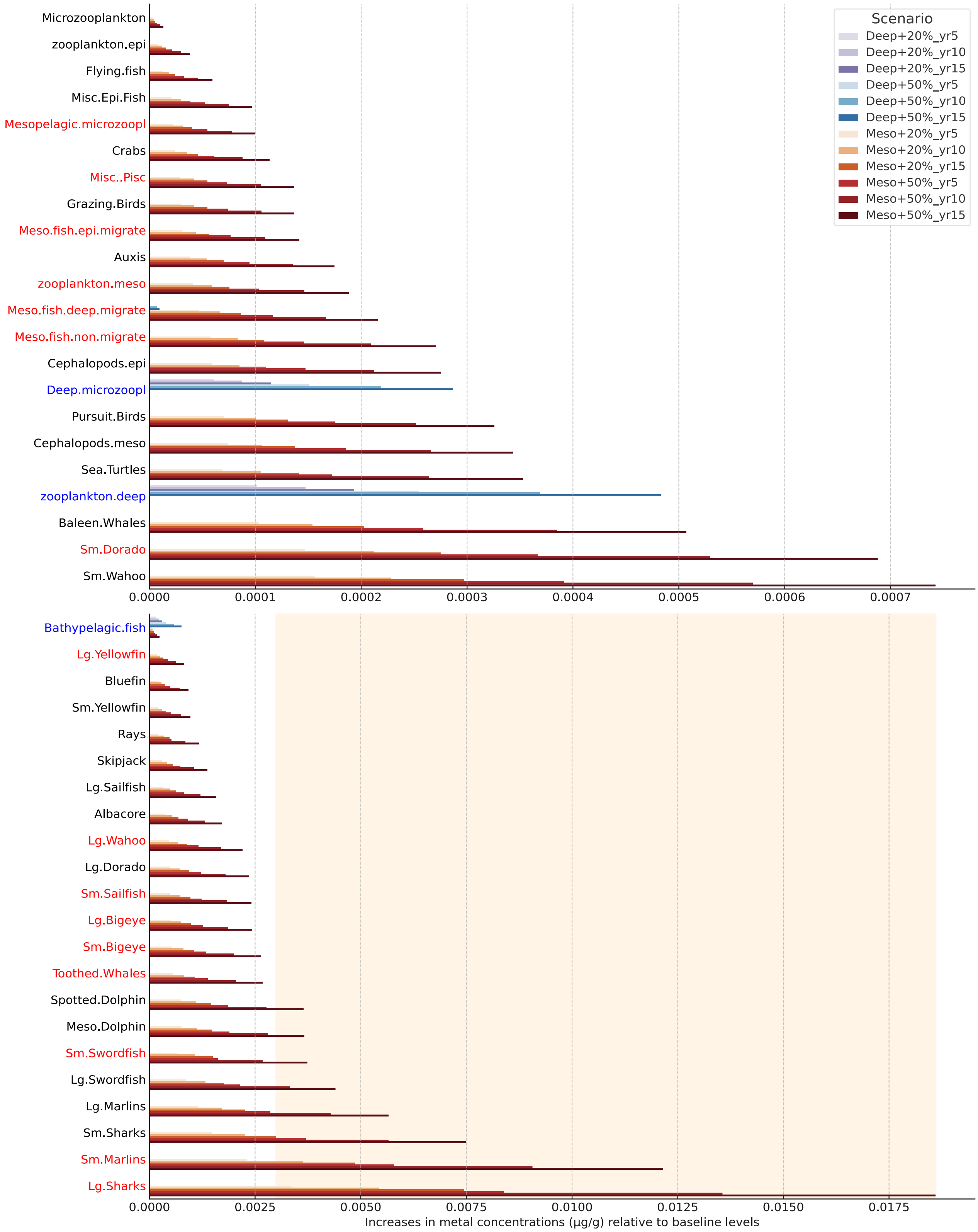

Figure 5. Relative increases in concentrations ($\mu g\ g^{-1}$) of metal group 1 after 5, 10 and 15 years across all consumer functional groups, under +20% and +50% baseline inflow concentrations in the mesopelagic (200–1,000 m) and bathypelagic (1,000–3,000 m) discharge scenarios. Taxa primarily feeding in epipelagic, mesopelagic and bathypelagic habitats are noted in black, red, and blue text. Yellow shading indicates medium level concentration increases of between 1% and 10% of the health advisory threshold for metal group one of 0.3 $\mu g\ g^{-1}$.

3.3 Model performance

Sensitivity coefficients were calculated for each taxa group under ±10% changes to four parameter categories: *Initial concentrations*, *Uptake rates*, *Elimination rates*, and *Metabolic decay rates* (Figure 6). Distinct variation in sensitivity magnitude was observed across both scenario types and taxa groups, with a clear gradient from lower to higher trophic levels. Changes in the background environmental concentrations demonstrate that the modelled metal concentrations in all functional groups are sensitive to seawater metal inputs with sensitivity coefficients reaching up to 0.11. This indicates and that simulated changes in seawater metal concentrations will result in proportional concentration changes in the taxa groups. Changes to initial metal concentrations of producers (detritus, phytoplankton and small producers) had minimal effect (sensitivity close to zero) of simulated concentrations in higher up consumers.

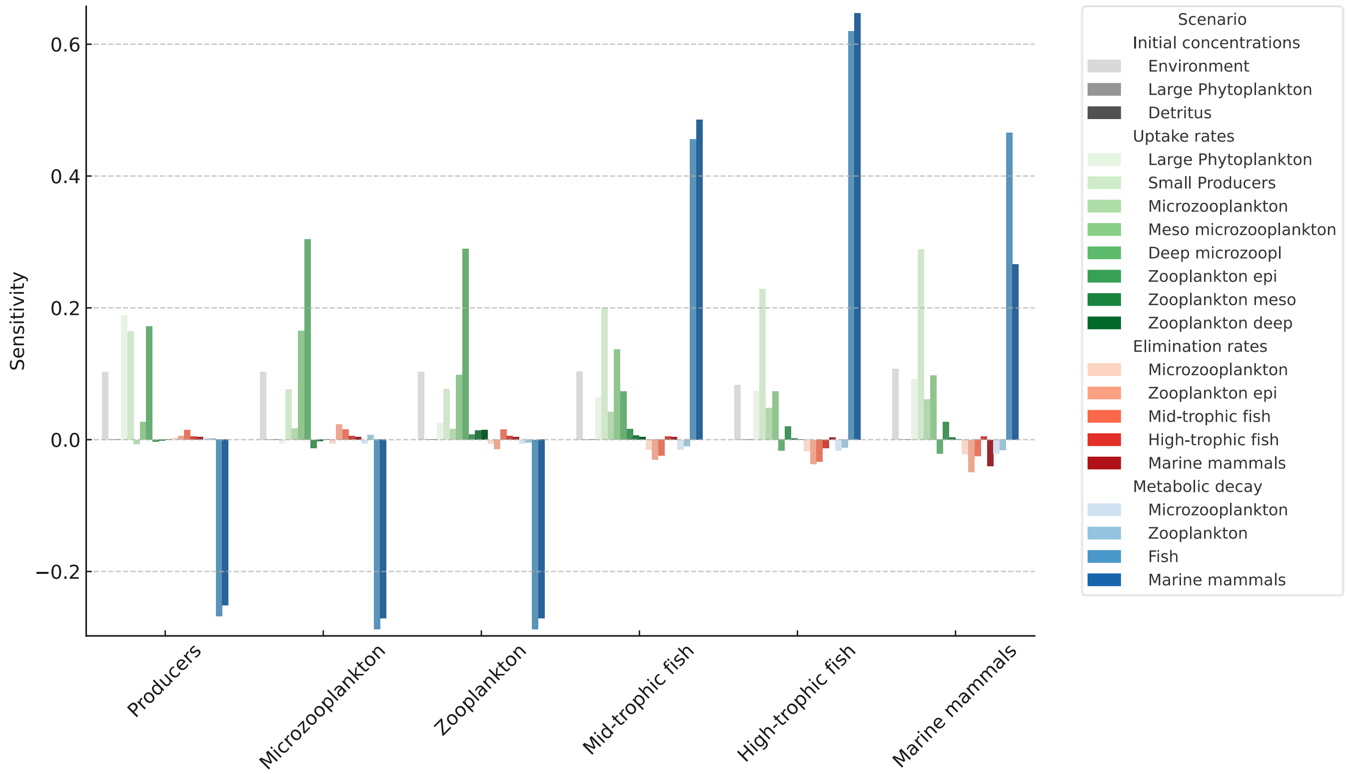

Figure 6. Sensitivity of simulated metal one concentrations in producers, zooplankton, fish and marine mammal taxa groups to each input parameter, as measured through the sensitivity coefficients. The bar heights represent the magnitude of sensitivity, while different colours indicate parameter changes to particular taxa groups.

Changes to uptake rates resulted in consistently high sensitivity values, especially for producers and microzooplankton, with peak responses linked to uptake by small producers and large phytoplankton. Mid-trophic fish were also sensitive to uptake changes in microzooplankton, whereas marine mammals and high-trophic fish showed low sensitivity across all uptake parameters. Under elimination rate changes, the strongest responses were observed in zooplankton and mid-trophic fish, particularly from meso- and microzooplankton elimination. Microzooplankton showed moderate sensitivity, while producers, high-trophic fish, and marine mammals were minimally affected. For metabolic decay, microzooplankton again exhibited the highest sensitivity, notably to meso- and microzooplankton-related parameters. Producers and zooplankton were also responsive, whereas mid- and high-trophic fish and marine mammals showed generally low sensitivity across this category.

3.4 Bioaccumulation

Model outputs, evaluated using the threshold-based bioaccumulation classification matrix, indicated a range of bioaccumulation concerns for metal group 1 across functional groups, with notable variation between mesopelagic and bathypelagic exposure scenarios (Figure 7). Notably, no group exceeded the high classification threshold of 0.03 $\mu g\ g^{-1}$ (10% of health advisory guidelines) under any modelled condition over the 20-year model run.

Under the bathypelagic exposure scenario, bioaccumulation levels were classified as non-detectable for most functional groups unless they were deep dwelling, where species such as bathypelagic fish had clearly detectable levels. No functional group exhibited medium or high bioaccumulation levels under any bathypelagic exposure scenario. In contrast, under the mesopelagic discharge scenario, five high-trophic pelagic taxa groups including marlins, sharks, toothed whales, dolphins, and large wahoo reached medium concern levels at the highest simulated concentration increase (+50% relative to baseline inflow rates). At intermediate exposure concentrations (+5% to +20%), only marlins and sharks retained medium concern classifications, while all groups shifted to detectable levels under minimal exposure (+5%), with concentrations remaining below 0.003 $\mu g\ g^{-1}$.

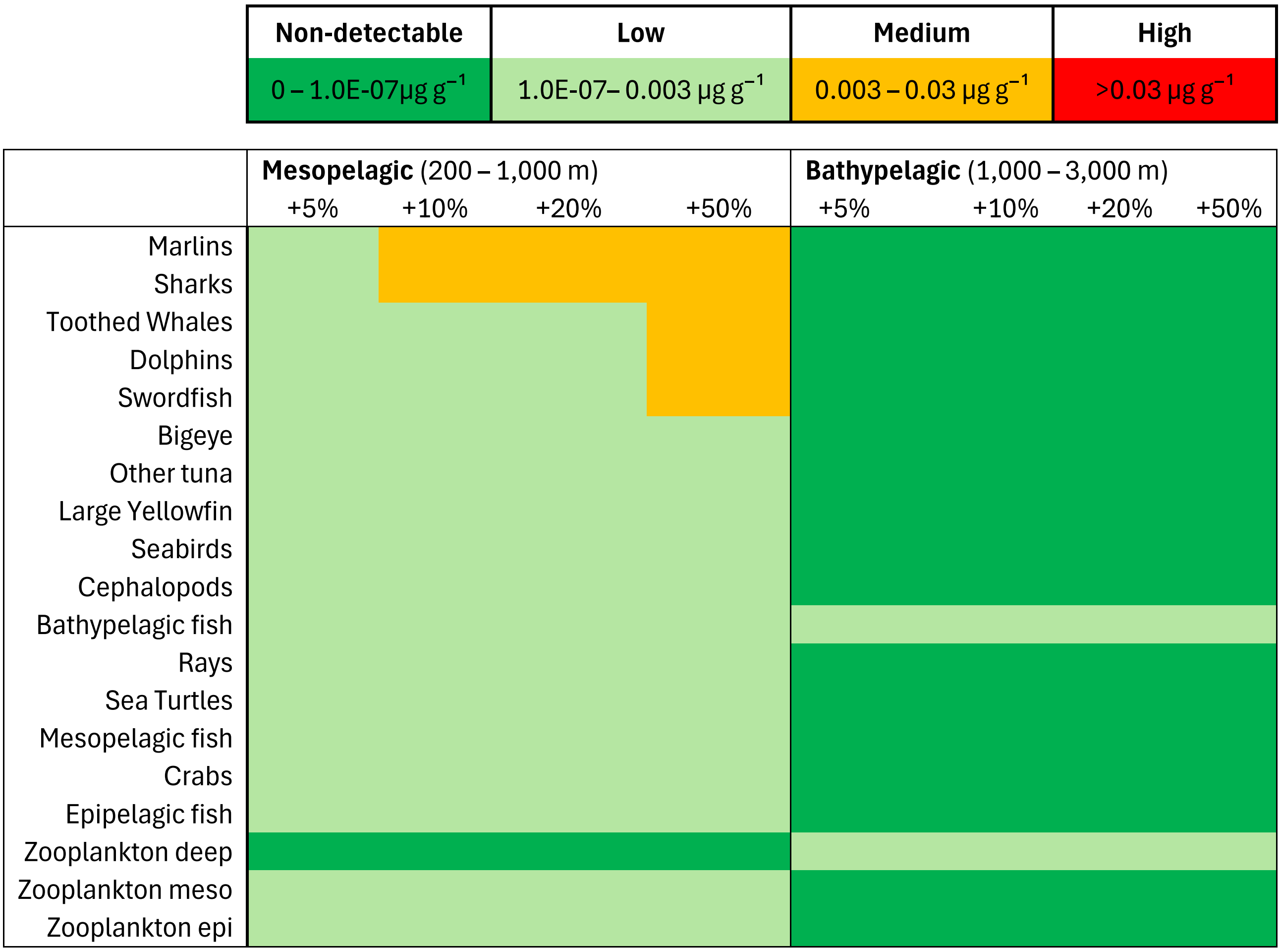

Figure 7. Classification of bioaccumulation based on model simulated increases in metal group 1 concentrations for functional groups under discharge exposure scenarios at mesopelagic and bathypelagic depths.

4 Discussion

This study presents a systematic assessment of how midwater sediment discharge plumes from deep-sea mining may interact with pelagic ecosystems. We used an updated Ecopath with Ecosim (EwE) and Ecotracer model framework that incorporates vertical habitat layers and functional diversity from epipelagic, mesopelagic and deep bathypelagic zones. Metal discharges were simulated across various depths and exposure intensities to assess food web-mediated transfer from potential mid-water discharge plumes to predators such as tuna and marine mammals.

Model results highlight that discharge depth, metal group type and concentration are critical in shaping exposure outcomes. Simulation of discharge plumes between 200–1,000 m in the mesopelagic zone led to more elevated metal concentrations across a wider range of functional groups and vertical habitats. This is attributed to the higher biological productivity and connectivity of the epipelagic and upper mesopelagic zones, where zooplankton and small mesopelagic fish, key prey for predators like tuna, are most abundant (Robison *et al*. 2010). In contrast, deeper discharge depths between 1,000–3,000 m resulted in more localized exposure, with bioaccumulation largely confined to deep-dwelling species and minimal (non-detectable) transfer to upper pelagic food web, in cases where small trophic linkages were represented.

Across all scenarios, bioaccumulation patterns followed expected trophic dynamics: producers and microzooplankton showed the greatest sensitivity to changes in uptake and elimination rates, while top predators were less responsive due to longer lifespans and lower turnover. Among metal groups, essential trace elements exhibited the highest relative increases, while more toxic and persistent metals, such as mercury-like compounds, accumulated at lower concentrations but posed greater biomagnification risks.

Elevated or prolonged exposure in the mesopelagic zone increased bioaccumulation in mesopelagic organisms, which represent an important dietary link between deep and epipelagic zones. This trophic pathway is particularly relevant given that tuna, sharks, and other high-order pelagic predators already exhibit elevated concentrations of toxic metals, largely to global atmospheric emissions and oceanic cycling. Observed concentrations in shark and tuna muscle typically range from 0.2 to 3.0 $\mu g\ g^{-1}$ WW, often exceeding international health advisory thresholds (*e.g.*, Amezcua *et al.* 2022; Médieu *et al.* 2021). In this context, our modelling suggests that realistic discharge scenarios, representing less than 5% additional loadings relative to existing environmental inputs, are unlikely to substantially increase contaminant levels in high-order predators, with predicted increases in tissue concentrations of highly toxic metals remaining below 1%.

Relative increases in contaminant concentrations under extremely high exposure scenarios (*e.g*., 50% above baseline inflow estimates) were modest when compared to the variability observed in natural input sources, supporting the ecological relevance of the predictions. For example, global fluxes of dissolved Fe to the ocean have been estimated at up to 1.81 Tg Fe yr^{-1} (Tagliabue *et al.*

2016), while atmospheric Hg contributions are approximately 1.9 Gg Hg yr^{-1} (Streets *et al.* 2011; Muntean *et al.* 2014). These benchmarks support the idea that midwater releases of mining discharge, at least at modelled levels, fall within existing biogeochemical loading ranges.

4.1 Key model assumptions and directions for future research

Our model results provide insight into depth-dependent exposure and trophic transfer potential, but its interpretation must be grounded in the underlying assumptions. The strength of its predictions depends on how accurately it represents ecological, chemical and physical complexity in the open ocean. Below, we outline four primary assumptions affecting exposure estimates and identify priorities for refining future ecosystem-based risk assessments:

Assumption 1: Uniform exposure across depths
We assume constant contaminant exposure within fixed depth layers, without representing dynamic plume behaviour such as dilution, advection, or vertical mixing. This simplification allows tractable analysis of discharge depth and intensity effects and offers a conservative basis for early risk assessment where high-resolution hydrodynamic data are lacking. However, it may overestimate exposure in areas where physical processes disperse contaminants (Aleynik *et al.* 2017; Ouillon *et al.* 2022; Peacock and Ouillon, 2023).

Integrating 3D oceanographic transport models or data-assimilative plume forecasts with ecosystem frameworks like EwE Ecospace could significantly improve spatial realism and site-specific risk precision.

Assumption 2: Simplified bioavailability and chemical speciation of metals
Metals were grouped into three broad categories, treating all as fully bioavailable and chemically equivalent. This facilitates comparison of trophic transfer patterns but omits metal-specific speciation, complexation, and particle-binding effects known to influence bioavailability and toxicity (Morel and Price, 2003; Sunda, 2012). For example, free ionic forms are typically more bioavailable than organically bound or particulate species.

While this generalisation is common in early-stage models, future iterations should incorporate speciation dynamics, especially for metals like mercury and copper, using empirical data and biogeochemical sub-models.

Assumption 3 Simplified vertical and biological structuring
To maintain tractability, the model omits vertical stratification, oxygen minimum zones, and biological processes such as microbial remineralisation and ontogenetic migration; all of which influence contaminant dynamics (Steinberg *et al.* 2000; Robison, 2003; Hannides *et al.* 2009; Hawco *et al.* 2016; Stanley *et al.* 2020; Orcutt *et al.* 2020). However, we include two hypothetical deep-dwelling fish groups to explore potential contaminant transfer below 1,000 m, acknowledging limited evidence of vertical migration or significant biomass below 800–1,000 m in the eastern Pacific (Ryan 2024; Perelman *et al.* 2025). These inclusions help test possible

connectivity between deep and epipelagic systems, particularly contaminant transfer via mesopelagic prey to predators such as tunas.

As these pathways remain uncertain, they represent critical knowledge gaps for future empirical and modelling efforts.

Assumption 4: Static food web, fisheries, and environmental conditions
The model assumes a fixed trophic structure without species migration, dietary shifts, or seasonal or climate-driven productivity changes. It also holds fisheries catches and primary productivity constant, thereby omitting potential interactions between fishing pressure, climate variability, and contaminant exposure. While this allows clearer scenario comparisons, it overlooks key ecological and environmental dynamics shown to influence pelagic systems (Watters *et al.* 2003; Preikshot *et al.* 2013).

Incorporating migratory behaviours, variable fishing effort, and seasonal or interannual environmental forcing and climate change scenarios would improve predictive capacity, especially where human health, market access, or catch quality may be affected.

These deliberate simplifications enabled the development of a tractable, scenario-based model to assess depth-dependent risks from deep-sea mining discharges. Although the model cannot capture the full dynamism of pelagic systems, it provides a foundation for evaluating contaminant pathways under plausible and extreme conditions. Future refinements should prioritise coupling with physical oceanographic models, integrating movement ecology, and enhancing metal-specific chemistry to support more robust, ecosystem-based risk assessments.

Overall, this study would support precautionary advice to avoid deep-sea mining generated discharges in the upper 1,000 m of the water column, where food web connectivity, productivity, and predator exposure are highest. Although discharges below 1,000 m show limited immediate transfer to pelagic predators, indirect exposure pathways (*e.g.*, via mesopelagic prey) remain unresolved and merit further attention.

References

Amano, M. and Yoshioka, M., 2003. Sperm whale diving behavior monitored using a suction-cup-attached TDR tag. *Marine ecology progress series*, *258*, pp.291-295.

Amezcua, F., Ruelas-Inzunza, J., Coiraton, C., Spanopoulos-Zarco, P. and Páez-Osuna, F., 2022. A global review of cadmium, mercury, and selenium in sharks: geographical patterns, baseline levels and human health implications. *Reviews of Environmental Contamination and Toxicology*, 260(1), p.4.

Amon, D.J., Gollner, S., Morato, T., Smith, C.R., Chen, C., Christiansen, S., Currie, B., Drazen, J.C., Fukushima, T., Gianni, M. and Gjerde, K.M., 2022. Assessment of scientific gaps related to the effective environmental management of deep-seabed mining. *Marine Policy*, *138*, p.105006.

Amon, D.J., Palacios-Abrantes, J., Drazen, J.C., Lily, H., Nathan, N., van der Grient, J.M. and McCauley, D., 2023. Climate change to drive increasing overlap between Pacific tuna fisheries and emerging deep-sea mining industry. *Ocean Sustainability*, *2*(1), p.9.

Aleynik, D., Inall, M. E., Dale, A. C., and Vink, A. (2017). The impact of remotely generated internal waves on sediment resuspension and deep benthic ecosystems. *Scientific Reports*, 7, 46350.

Arnot, J.A. and Gobas, F.A., 2004. A food web bioaccumulation model for organic chemicals in aquatic ecosystems. *Environmental Toxicology and Chemistry*, *23*(10), pp.2343-2355.

Balistrieri, L., Brewer, P.G. and Murray, J.W., 1981. Scavenging residence times of trace metals and surface chemistry of sinking particles in the deep ocean. *Deep Sea Research Part A. Oceanographic Research Papers*, *28*(2), pp.101-121.

Bruland, K.W. and Lohan, M.C., 2006. Controls of trace metals in seawater. *Treatise on geochemistry*, *6*, pp.23-47.

Choy, C.A., Wabnitz, C.C., Weijerman, M., Woodworth-Jefcoats, P.A. and Polovina, J.J., 2016. Finding the way to the top: how the composition of oceanic mid-trophic micronekton groups determines apex predator biomass in the central North Pacific. *Marine Ecology Progress Series*, *549*, pp.9-25.

Christensen, V., Walters, C.J. and Pauly, D., 2005. Ecopath with Ecosim: a user's guide. *Fisheries Centre, University of British Columbia, Vancouver*, *154*, p.31.

Christiansen, B., Denda, A. and Christiansen, S., 2020. Potential effects of deep seabed mining on pelagic and benthopelagic biota. *Marine Policy*, *114*, p.103442.

Colléter, M., Valls, A., Guitton, J., Gascuel, D., Pauly, D. and Christensen, V., 2015. Global overview of the applications of the Ecopath with Ecosim modeling approach using the EcoBase models repository. *Ecological Modelling*, *302*, pp.42-53.

Craig, J.K. and Link, J.S., 2023. It is past time to use ecosystem models tactically to support ecosystem-based fisheries management: Case studies using Ecopath with Ecosim in an operational management context. *Fish and Fisheries*, *24*(3), pp.381-406.

Dambacher, J.M., Young, J.W., Olson, R.J., Allain, V., Galván-Magaña, F., Lansdell, M.J., Bocanegra-Castillo, N., Alatorre-Ramírez, V., Cooper, S.P. and Duffy, L.M., 2010. Analyzing pelagic food webs leading to top predators in the Pacific Ocean: a graph-theoretic approach. *Progress in Oceanography*, *86*(1-2), pp.152-165.

De Laender, F., Morselli, M., Baveco, H., Van den Brink, P.J. and Di Guardo, A., 2015. Theoretically exploring direct and indirect chemical effects across ecological and exposure scenarios using mechanistic fate and effects modelling. *Environment international*, *74*, pp.181-190.

Drazen, J., Smith, C., Gjerde, K., Au, W., Black, J., Carter, G., Clark, M., Durden, J., Dutrieux, P., Goetze, E. and Haddock, S., 2019a. Report of the workshop Evaluating the nature of midwater mining plumes and their potential effects on midwater ecosystems. *Research Ideas and Outcomes*, *5*, p.e33527.

Drazen, J.C., Leitner, A.B., Morningstar, S., Marcon, Y., Greinert, J. and Purser, A., 2019b. Observations of deep-sea fishes and mobile scavengers from the abyssal DISCOL experimental mining area. *Biogeosciences*, *16*(16), pp.3133-3146.

Drazen, J.C., Smith, C.R., Gjerde, K.M., Haddock, S.H., Carter, G.S., Choy, C.A., Clark, M.R., Dutrieux, P., Goetze, E., Hauton, C. and Hatta, M., 2020. Midwater ecosystems must be considered when evaluating environmental risks of deep-sea mining. *Proceedings of the National Academy of Sciences*, *117*(30), pp.17455-17460.

Duffy, L.M., Kuhnert, P.M., Pethybridge, H.R., Young, J.W., Olson, R.J., Logan, J.M., Goñi, N., Romanov, E., Allain, V., Staudinger, M.D. and Abecassis, M., 2017. Global trophic ecology of yellowfin, bigeye, and albacore tunas: understanding predation on micronekton communities at ocean-basin scales. *Deep Sea Research Part II: Topical Studies in Oceanography*, *140*, pp.55-73.

Ferriss, B.E. and Essington, T.E., 2014. Does trophic structure dictate mercury concentrations in top predators? A comparative analysis of pelagic food webs in the Pacific Ocean. *Ecological Modelling*, *278*, pp.18-28.

Fitzsimmons, J.N., Conway, T.M., Lee, J.M., Kayser, R., Thyng, K.M., John, S.G. and Boyle, E.A., 2016. Dissolved iron and iron isotopes in the southeastern Pacific Ocean. *Global Biogeochemical Cycles*, *30*(10), pp.1372-1395.

Fitzsimmons, J.N., Gunnells S., Morton, P., Kubler-Dudgeon, I., Adamczyk, K., Larrouilh, C., and Toczek, J., 2025. Texas A&M Pelagic Chemical Oceanography (Dissolved) Task 7: Characterize Trace metals, nutrients, and water column chemistry, Work Package 004: Pelagic Collector Test. Final Collector Test Report to The Metals Company 10/05/2025

Gobas, F.A.P.C. and Morrison, H.A., 2000. Bioconcentration and biomagnification in the aquatic environment. *Handbook of property estimation methods for chemicals*, pp.189-231.

Godinot, O. and Allain, V., 2003. A preliminary Ecopath model of the warm pool pelagic ecosystem. EcoBase: https://ecobase.ecopath.org/ Accessed 29/11/2023.

Hannides, C.C., Landry, M.R., Benitez-Nelson, C.R., Styles, R.M., Montoya, J.P. and Karl, D.M., 2009. Export stoichiometry and migrant-mediated flux of phosphorus in the North Pacific Subtropical Gyre. *Deep Sea Research Part I: Oceanographic Research Papers*, *56*(1), pp.73-88.

Heymans, J.J., Coll, M., Link, J.S., Mackinson, S., Steenbeek, J., Walters, C. and Christensen, V., 2016. Best practice in Ecopath with Ecosim food-web models for ecosystem-based management. *Ecological modelling*, *331*, pp.173-184.

Hatje, V., Lamborg, C.H. and Boyle, E.A., 2018. Trace-metal contaminants: human footprint on the ocean. *Elements: An International Magazine of Mineralogy, Geochemistry, and Petrology*, *14*(6), pp.403-408.

Hawco, N.J., Ohnemus, D.C., Resing, J.A., Twining, B.S. and Saito, M.A., 2016. A dissolved cobalt plume in the oxygen minimum zone of the eastern tropical South Pacific. *Biogeosciences*, *13*(20), pp.5697-5717.

Hoover, C., Giraldo, C., Ehrman, A., Suchy, K.D., Macphee, S.A., Brewster, J., Reist, J.D., Power, M., Swanson, H. and Loseto, L., 2021. The Canadian Beaufort Shelf trophic structure: evaluating an ecosystem modelling approach by comparison with observed stable isotopic structure. *Arctic Science*, *8*(1), pp.292-312.

Irigoien, X., Klevjer, T.A., Røstad, A., Martinez, U., Boyra, G., Acuña, J.L., Bode, A., Echevarria, F., Gonzalez-Gordillo, J.I., Hernandez-Leon, S. and Agusti, S., 2014. Large mesopelagic fishes biomass and trophic efficiency in the open ocean. *Nature communications*, *5*(1), p.3271.

Jochum KP, Nohl U., Herwig, K., Lammel, E., Stoll, B., and Hofmann, A.B., 2005 GeoReM – A new Geochemical Database for Reference materials and isotope standards. Geostandards and Geoanalytical Research 29,3, 333-338. Available from: https://georem.mpch-mainz.gwdg.de [Accessed 23 June 2025].

Keramidas, I., Dimarchopoulou, D., Ofir, E., Scotti, M., Tsikliras, A.C. and Gal, G., 2023. Ecotrophic perspective in fisheries management: a review of Ecopath with Ecosim models in European marine ecosystems. *Frontiers in Marine Science*, *10*, p.1182921.

Li, M.L., Gillies, E.J., Briner, R., Hoover, C.A., Sora, K.J., Loseto, L.L., Walters, W.J., Cheung, W.W. and Giang, A., 2022. Investigating the dynamics of methylmercury bioaccumulation in the Beaufort Sea shelf food web: a modeling perspective. *Environmental Science: Processes & Impacts*, *24*(7), pp.1010-1025.

Link, J.S., 2010. Adding rigor to ecological network models by evaluating a set of pre-balance diagnostics: a plea for PREBAL. *Ecological modelling*, *221*(12), pp.1580-1591.

McMullen, K., Vargas, F.H., Calle, P., Alavarado-Cadena, O., Pakhomov, E.A. and Alava, J.J., 2024. Modelling microplastic bioaccumulation and biomagnification potential in the Galápagos penguin ecosystem using Ecopath and Ecosim (EwE) with Ecotracer. *PLoS One*, *19*(1), p.e0296788.

Mathews, T., Fisher, N.S., Jeffree, R.A. and Teyssié, J.L., 2008. Assimilation and retention of metals in teleost and elasmobranch fishes following dietary exposure. *Marine Ecology Progress Series*, *360*, pp.1-12.

Miller, K.A., Thompson, K.F., Johnston, P. and Santillo, D., 2018. An overview of seabed mining including the current state of development, environmental impacts, and knowledge gaps. *Frontiers in Marine Science*, *4*, p.312755.

Médieu, A., Point, D., Receveur, A., Gauthier, O., Allain, V., Pethybridge, H., Menkes, C.E., Gillikin, D.P., Revill, A.T., Somes, C.J. and Collin, J., 2021. Stable mercury concentrations of tropical tuna in the south western Pacific ocean: An 18-year monitoring study. *Chemosphere*, *263*, p.128024.

Moore, J.K. and Braucher, O., 2007. Observations of dissolved iron concentrations in the World Ocean: implications and constraints for ocean biogeochemical models. *Biogeosciences Discussions*, *4*(2), pp.1241-1277.

Morel, F.M.M., and Price, N.M. (2003). *The biogeochemical cycles of trace metals in the oceans.* Science, 300(5621), 944–947. https://doi.org/10.1126/science.1083545

Munson, K.M., Lamborg, C.H., Swarr, G.J. and Saito, M.A., 2015. Mercury species concentrations and fluxes in the Central Tropical Pacific Ocean. *Global Biogeochemical Cycles*, *29*(5), pp.656-676.

Muntean, M.; Janssens-Maenhout, G.; Song, S.; Selin, N. E.; Olivier, J. G. J.; Guizzardi, D.; Maas, R.; Dentener, R. Trend Analysis from 1970 to 2008 and Model Evaluation of EDGARv4 Global Gridded Anthropogenic Mercury Emissions. *Sci. Total Environ.* **2014**, *494–495*, 337– 350.

Myriokefalitakis, S., Ito, A., Kanakidou, M., Nenes, A., Krol, M.C., Mahowald, N.M., Scanza, R.A., Hamilton, D.S., Johnson, M.S., Meskhidze, N. and Kok, J.F., 2018. Reviews and syntheses: the GESAMP atmospheric iron deposition model intercomparison study. *Biogeosciences*, *15*(21), pp.6659-6684.

Olson, R.J., and Watters, G.M. 2003. A model of the pelagic ecosystem in the eastern tropical Pacific Ocean. Inter-Am. Trop. Tuna Comm. Bull. 22: 133–218.

Olson, R.J., Duffy, L.M., Kuhnert, P.M., Galvan-Magana, F., Bocanegra-Castillo, N. and Alatorre-Ramirez, V., 2014. Decadal diet shift in yellowfin tuna Thunnus albacares suggests broad-scale food web changes in the eastern tropical Pacific Ocean. *Marine Ecology Progress Series*, *497*, pp.157-178.

Orcutt, B.N., Bradley, J.A., Brazelton, W.J., Estes, E.R., Goordial, J.M., Huber, J.A., Jones, R.M., Mahmoudi, N., Marlow, J.J., Murdock, S. and Pachiadaki, M., 2020. Impacts of deep-sea mining on microbial ecosystem services. *Limnology and Oceanography*, *65*(7), pp.1489-1510.

Ouillon, R., Muñoz-Royo, C., Alford, M.H. and Peacock, T., 2022. Advection-diffusion-settling of deep-sea mining sediment plumes. Part 1: Midwater plumes. *Flow*, *2*, p.E22.

Peacock, T. and Ouillon, R., 2023. The fluid mechanics of deep-sea mining. *Annual Review of Fluid Mechanics*, *55*(1), pp.403-430.

Perelman, J.N., Assad, V.E., Ladroit, Y., Escobar-Flores, P.C., Lindsay, D.J., Bergman, L.A. and Drazen, J.C., 2025. A multi-method assessment of pelagic communities in the remote eastern Pacific Ocean. *Elementa: Science of the Anthropocene*, *13*(1).

Preikshot, D., Beamish, R.J. and Neville, C.M., 2013. A dynamic model describing ecosystem-level changes in the Strait of Georgia from 1960 to 2010. *Progress in Oceanography*, *115*, pp.28-40.

Robison, B.H. (2003). What drives the diel vertical migrations of mesopelagic animals? *Journal of Experimental Marine Biology and Ecology,* 300(1-2), 79–95.

Rohal, M., Ainsworth, C., Lupher, B., Montagna, P.A., Paris, C.B., Perlin, N., Suprenand, P.M. and Yoskowitz, D., 2020. The effect of the Deepwater Horizon oil spill on two ecosystem services in the Northern Gulf of Mexico. *Environmental Modelling & Software*, *133*, p.104793.

Rose, K.A., Allen, J.I., Artioli, Y., Barange, M., Blackford, J., Carlotti, F., Cropp, R., Daewel, U., Edwards, K., Flynn, K. and Hill, S.L., 2010. End-to-end models for the analysis of marine ecosystems: challenges, issues, and next steps. *Marine and Coastal Fisheries*, *2*(1), pp.115-130.

Ryan T. 2024. Review of data obtained from Clipperton Zone acoustic observation project. Interim Report. CSIRO Marine Laboratories, Hobart.

Sandberg, J., Kumblad, L. and Kautsky, U., 2007. Can ECOPATH with ECOSIM enhance models of radionuclide flows in food webs? an example for 14C in a coastal food web in the Baltic Sea. *Journal of environmental radioactivity*, *92*(2), pp.96-111.

Sohrin, Y. and Bruland, K.W., 2011. Global status of trace elements in the ocean. *TrAC Trends in Analytical Chemistry*, *30*(8), pp.1291-1307.

Stanley, Z., Bachman, S.D. and Grooms, I., 2020. Vertical structure of ocean mesoscale eddies with implications for parameterizations of tracer transport. *Journal of Advances in Modeling Earth Systems*, *12*(10), p.e2020MS002151.

Starr, L.D., He, Y., Mason, R.P., Hammerschmidt, C.R., Newell, S.E. and Lamborg, C.H., 2025. Mercury distribution and speciation along the US GEOTRACES GP15 Pacific meridional transect. *Journal of Geophysical Research: Oceans*, *130*(4), p.2024JC021672.

Steinberg, D.K., Van Mooy, B.A., Buesseler, K.O., Boyd, P.W., Kobari, T. and Karl, D.M., 2008. Bacterial vs. zooplankton control of sinking particle flux in the ocean's twilight zone. *Limnology and Oceanography*, *53*(4), pp.1327-1338.

Stock, A., Murray, C.C., Gregr, E.J., Steenbeek, J., Woodburn, E., Micheli, F., Christensen, V. and Chan, K.M., 2023. Exploring multiple stressor effects with Ecopath, Ecosim, and Ecospace: Research designs, modeling techniques, and future directions. *Science of the Total Environment*, *869*, p.161719.

Streets, D. G.; Devane, M. K.; Lu, Z.; Bond, T. C.; Sunderland, E. M.; Jacob, D. J., 2011. All-Time Releases of Mercury to the Atmosphere from Human Activities. *Environ. Sci. Technol., 45* (24), 10485– 10491, DOI: 10.1021/es202765m

Sunda, W.G. (2012). Feedback interactions between trace metal nutrients and phytoplankton in the ocean. *Frontiers in Microbiology,* 3, 204. https://doi.org/10.3389/fmicb.2012.00204

Sweere, T.C., Dickson, A.J. and Vance, D., 2023. Nickel and zinc micronutrient availability in Phanerozoic oceans. *Gebiology,* 21, p.310-322. https://doi.org/10.1111/gbi.12541

Tagliabue, A., Aumont, O., DeAth, R., Dunne, J.P., Dutkiewicz, S., Galbraith, E., Misumi, K., Moore, J.K., Ridgwell, A., Sherman, E. and Stock, C., 2016. How well do global ocean biogeochemistry models simulate dissolved iron distributions?. *Global Biogeochemical Cycles*, *30*(2), pp.149-174.

Van Der Grient, J.M.A. and Drazen, J.C., 2021. Potential spatial intersection between high-seas fisheries and deep-sea mining in international waters. *Marine Policy*, *129*, p.104564.

von Hellfeld, R., Gade, C., Koppel, D.J., Walters, W.J., Kho, F. and Hastings, A., 2023. An approach to assess potential environmental mercury release, food web bioaccumulation, and human dietary methylmercury uptake from decommissioning offshore oil and gas infrastructure. *Journal of Hazardous Materials*, *452*, p.131298.

Walters, W.J. and Christensen, V., 2018. Ecotracer: analyzing concentration of contaminants and radioisotopes in an aquatic spatial-dynamic food web model. *Journal of Environmental Radioactivity*, *181*, pp.118-127.

Wang, W.X., 2002. Interactions of trace metals and different marine food chains. *Marine Ecology Progress Series*, *243*, pp.295-309.

Watters, G.M., Olson, R.J., Francis, R.C., Fiedler, P.C., Polovina, J.J., Reilly, S.B., Aydin, K.Y., Boggs, C.H., Essington, T.E., Walters, C.J. and Kitchell, J.F., 2003. Physical forcing and the dynamics of the pelagic ecosystem in the eastern tropical Pacific: simulations with ENSO-scale and global-warming climate drivers. *Canadian Journal of Fisheries and Aquatic Sciences*, *60*(9), pp.1161-1175.

Xu, Y., Wang, W.X. and Hsieh, D.P., 2001. Influences of metal concentration in phytoplankton and seawater on metal assimilation and elimination in marine copepods. *Environmental toxicology and chemistry*, *20*(5), pp.1067-1077.

Zhang, Y., Zhang, P., Song, Z., Huang, S., Yuan, T., Wu, P., Shah, V., Liu, M., Chen, L., Wang, X. and Zhou, J., 2023. An updated global mercury budget from a coupled atmosphere-land-ocean model: 40% more re-emissions buffer the effect of primary emission reductions. *One Earth*, *6*(3), pp.316-325.

Appendix A Supplementary material

A.1.1 Health advisory guideline thresholds for metals in seawater and seafood

App. Table A.1. Summary of international health advisory limits and guidelines for different metals in seawater and seafood assessed in this study.

	Seawater				Seafood			
	EU (µg/L)	EPA (µg/L)	WHO	ANZECC (µg/L)	EU ($\mu g\, g^{-1}$)	FDA ($\mu g\, g^{-1}$)	WHO/FAO ($\mu g\, g^{-1}$)	ANZFS ($\mu g\, g^{-1}$)
Mercury (Hg)	0.07	0.012	0.006	0.1	0.5	1	0.5	1
Lead (Pb)	0.04	8	10	3	0.3	0.5	0.3	0.5
Cadmium (Cd)	0.05	0.25	3	0.25	0.05	0.05	0.05	0.05
Nickel (Ni)	0.5	8.3	0.07	3	1	1	1	1
Zinc (Zn)	2	120	5	30	50	50	50	50
Manganese (Mn)	50	1,000	0.1	10	1	1	1	1
Copper (Cu)	0.05	3.1	2	1.3	30	30	30	30
Iron (Fe)	100	1,000	0.3	30	50	50	50	50
Aluminium (Al)	0.1	87	0.1	0.3	30	30	30	30
Cobalt (Co)	0.3	1.7	NA	0.7	NA	NA	NA	NA

A.1.2 Ecotracer parameters for different metal categories

App. Table A.2. Input parameters used for the Ecotracer models to represent three metal groups: M1 – Metal group 1, includes transition metals that bioaccumulate and are highly toxic (*e.g.*, Cd, Pb and Hg); M2 – Metal group 2 includes Zn, Ni, Mn and Cu; M3 – Metal group 3 includes essential elements such as Fe and Co.

	Direct absorption	Physical decay rate (y-1)			Proportion excreted			Metabolic decay (y-1)
		M1	M2	M3	M1	M2	M3	
Seabirds	0	0	0.01	0.02	0.15	0.3	0.4	29.02
Baleen Whales	0	0	0.01	0.02	0.15	0.3	0.4	0.70
Toothed Whales	0	0	0.01	0.02	0.15	0.3	0.4	0.80
Sea Turtles	0	0	0.01	0.02	0.15	0.3	0.4	0.33
Yellowfin	0	0	0.01	0.02	0.15	0.3	0.4	0.84
Bigeye	0	0	0.01	0.02	0.15	0.3	0.4	0.08
Marlins	0	0	0.01	0.02	0.15	0.3	0.4	0.06
Swordfish	0	0	0.01	0.02	0.15	0.3	0.4	0.03
Other Lrg Epi Fish	0	0	0.01	0.02	0.15	0.3	0.4	0.18
Sharks & Rays	0	0	0.01	0.02	0.15	0.3	0.4	0.06
Skipjack	0	0	0.01	0.02	0.15	0.3	0.4	0.38
Albacore	0	0	0.01	0.02	0.15	0.3	0.4	0.66
Auxis	0	0	0.01	0.02	0.15	0.3	0.4	4.14
Bluefin	0	0	0.01	0.02	0.15	0.3	0.4	0.08
Misc. Pisc	0	0	0.01	0.02	0.15	0.3	0.4	4.14
Flying Fish	0	0	0.01	0.02	0.15	0.3	0.4	0.82
Misc Epi Fish	0	0	0.01	0.02	0.15	0.3	0.4	0.80
Mesopelagic Fish	0	0	0.01	0.02	0.15	0.3	0.4	1.50
Bathypelagic Fish	0	0	0.01	0.02	0.15	0.3	0.4	0.20
Cephalopods	0	0	0.01	0.02	0.15	0.3	0.4	0.90
Crabs	0	0	0.01	0.02	0.15	0.3	0.4	1.60
Zooplankton	0.05	0	0.01	0.02	0.15	0.2	0.3	2.36
Microzooplankton	0.1	0	0.01	0.02	0.1	0.2	0.3	6.60
Primary producers	0.2	0	0.01	0.02	0	0	0	0
Detritus	0	0	0.01	0.02	0	0	0	0

A.1.3 Simulated concentrations for whole ecosystem and depth scenarios

App. Figure A.1. Model simulated concentrations ($\mu g\ g^{-1}$) in metal group one (highly toxic metals that bioaccumulate such as lead, cadmium and mercury) in functional groups over a 20-year simulation period after a 10 year burn-in period after which concentrations stabilised. Solid lines represent baseline concentrations under natural input conditions into the whole model ecosystem (black), into the mesopelagic zone (200–1,000 m, in red) and into the bathypelagic zone (1,000–3,000 m, in blue). Dotted lines represent scenarios with a 50% increase in metal inflow simulate contamination from a potential deep-sea mining mid-water plume discharge. Pink shading indicates concentrations exceeding the international health advisory threshold of 0.3 $\mu g\ g^{-1}$.

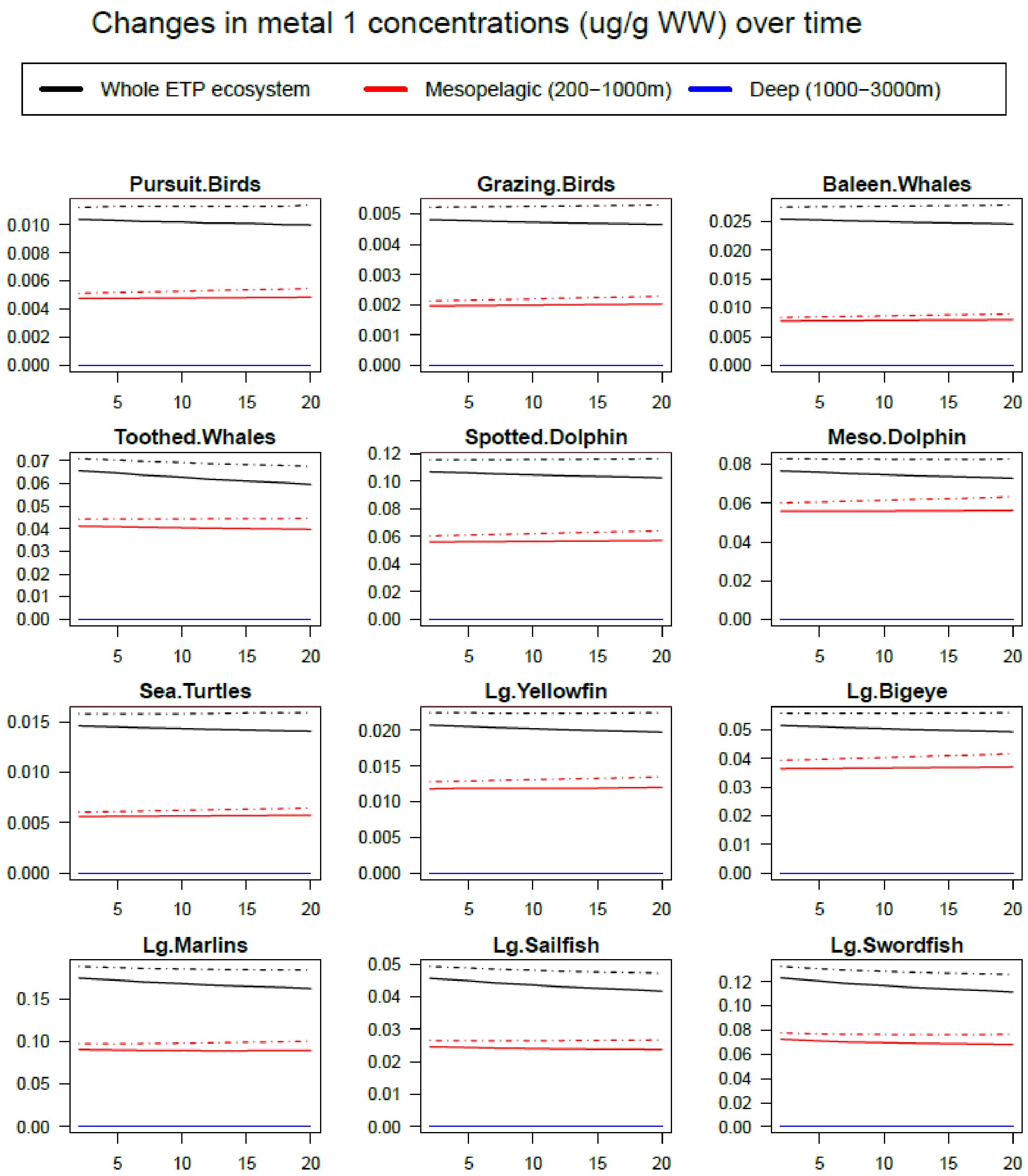

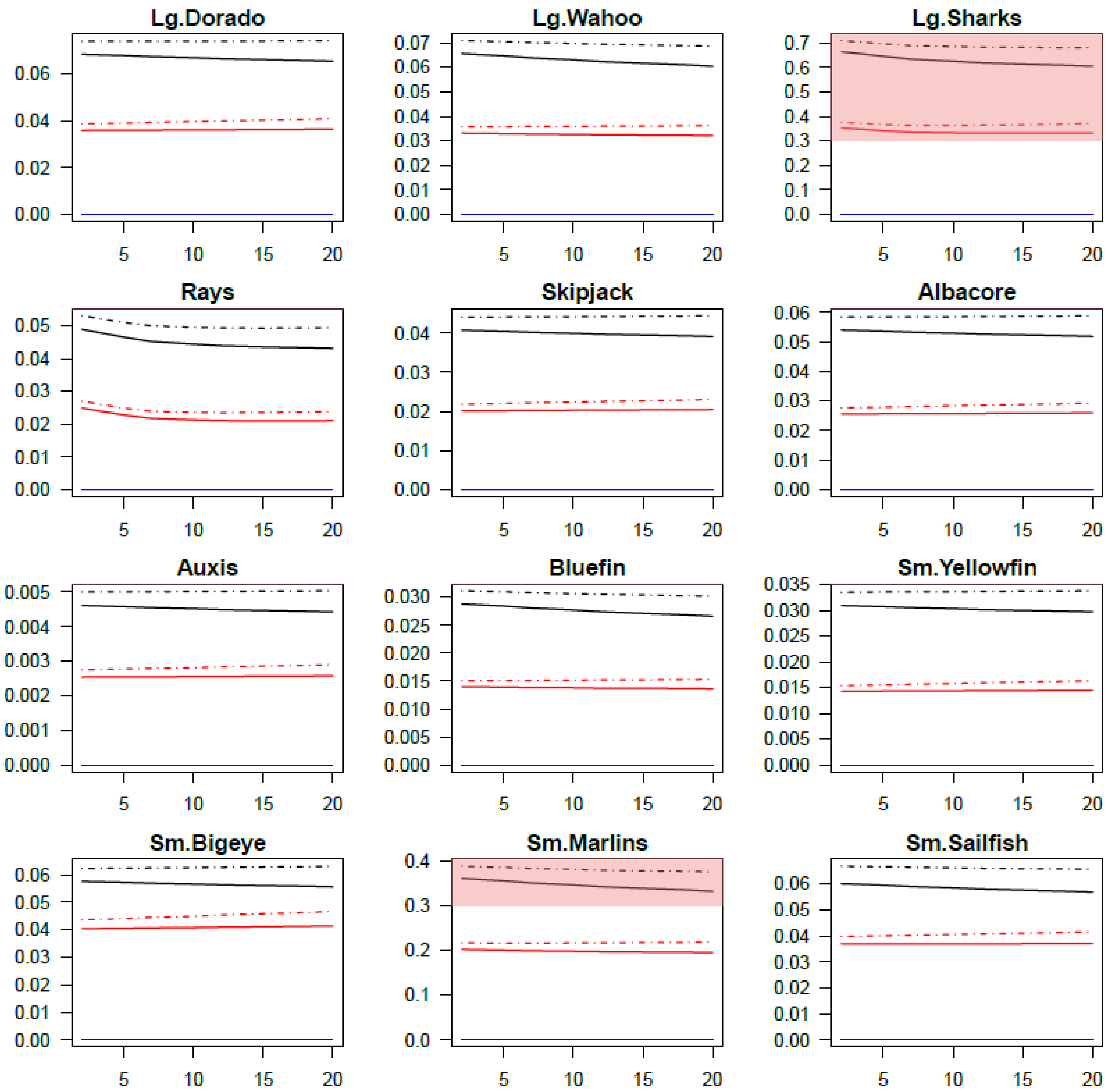
Lg.Dorado
Lg.Wahoo
Lg.Sharks
Rays
Skipjack
Albacore
Auxis
Bluefin
Sm.Yellowfin
Sm.Bigeye
Sm.Marlins
Sm.Sailfish

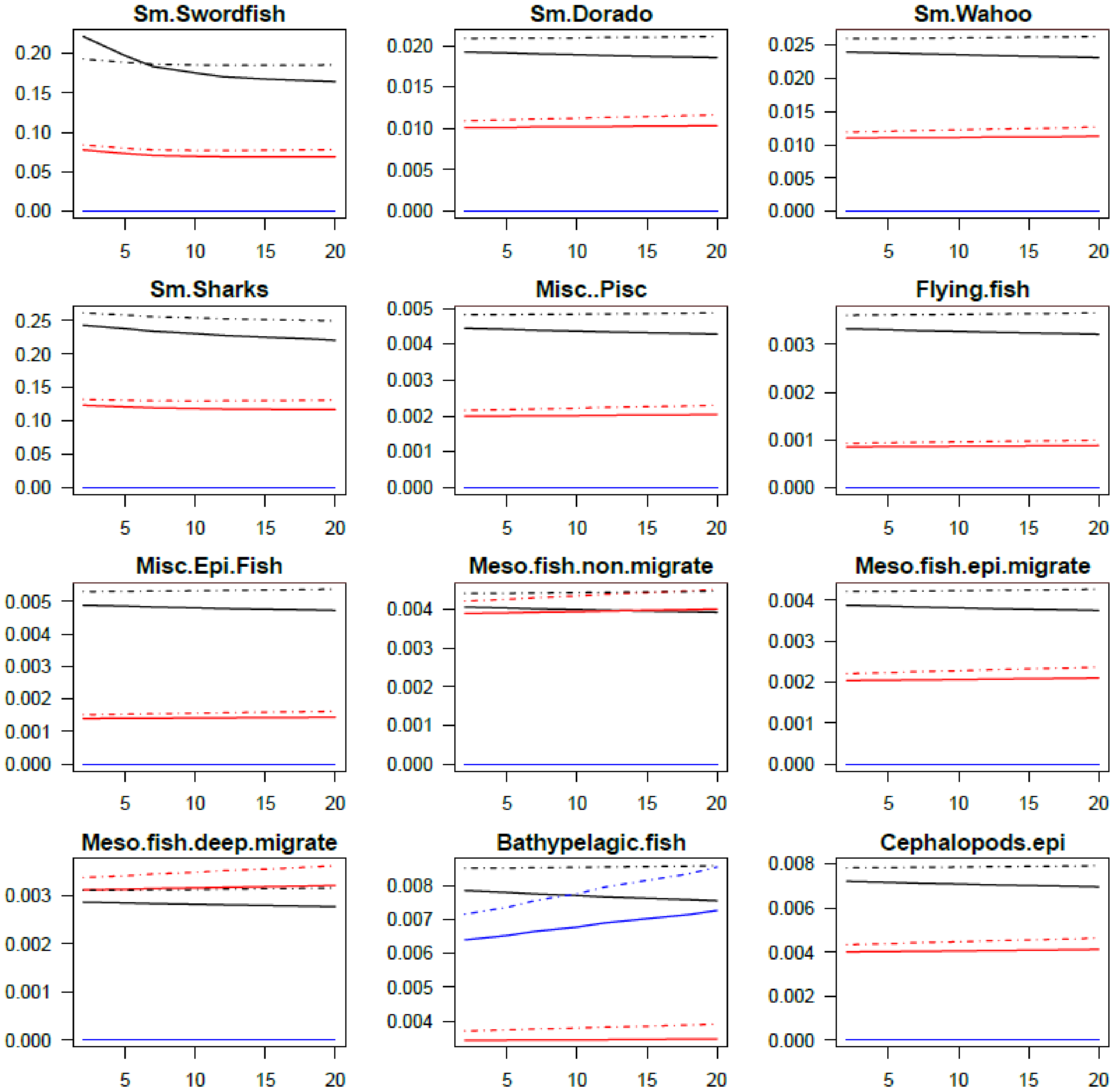
Sm.Swordfish
Sm.Dorado
Sm.Wahoo
Sm.Sharks
Misc..Pisc
Flying.fish
Misc.Epi.Fish
Meso.fish.non.migrate
Meso.fish.epi.migrate
Meso.fish.deep.migrate
Bathypelagic.fish
Cephalopods.epi
5
10
15
20

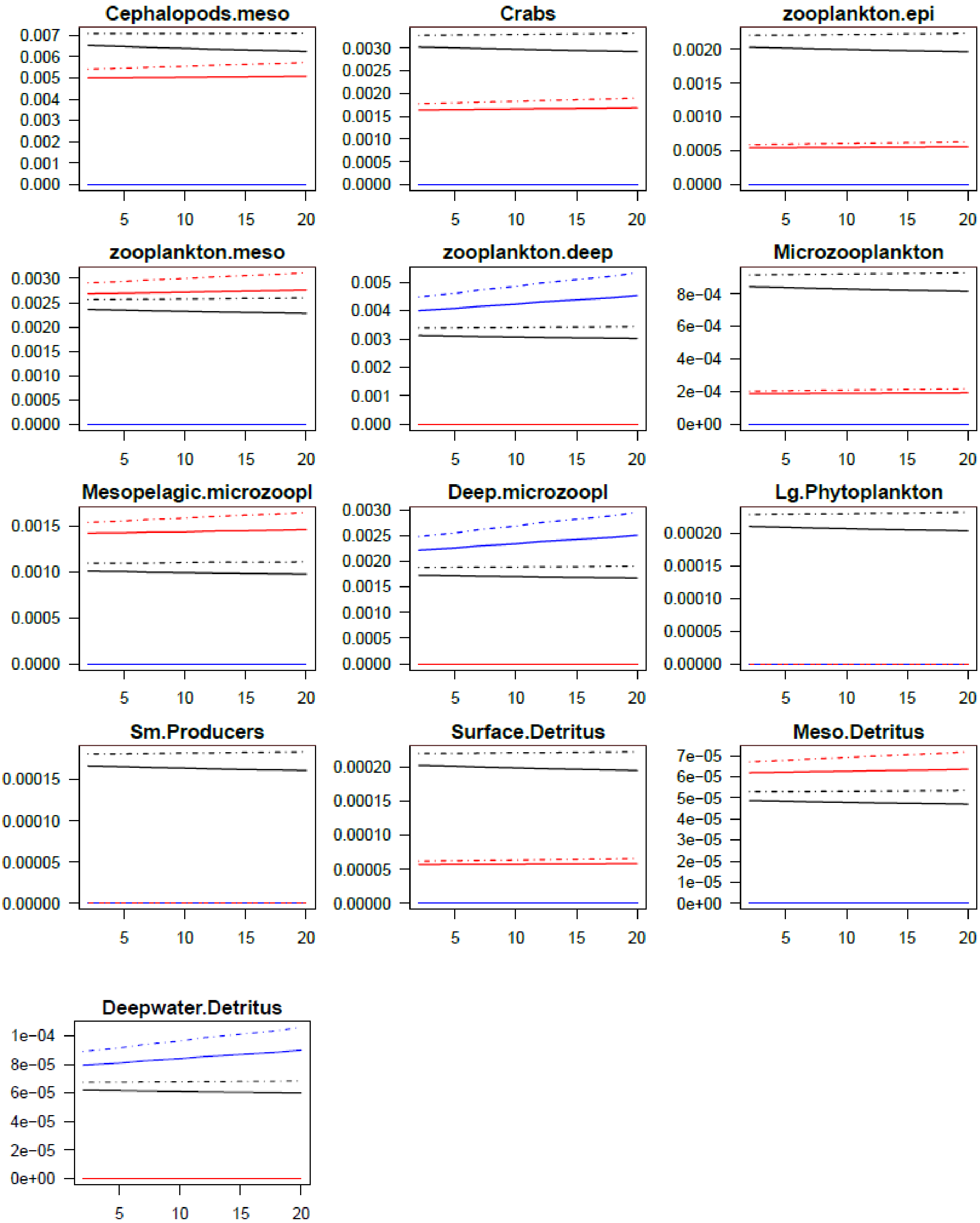
Cephalopods.meso
0.007
0.006
0.005
0.004
0.003
0.002
0.001
0.000
Crabs
0.0030
0.0025
0.0020
0.0015
0.0010
0.0005
0.0000
zooplankton.epi
0.0020
0.0015
0.0010
0.0005
0.0000
zooplankton.meso
0.0030
0.0025
0.0020
0.0015
0.0010
0.0005
0.0000
zooplankton.deep
0.005
0.004
0.003
0.002
0.001
0.000
Microzooplankton
8e−04
6e−04
4e−04
2e−04
0e+00
Mesopelagic.microzoopl
0.0015
0.0010
0.0005
0.0000
Deep.microzoopl
0.0030
0.0025
0.0020
0.0015
0.0010
0.0005
0.0000
Lg.Phytoplankton
0.00020
0.00015
0.00010
0.00005
0.00000
Sm.Producers
0.00015
0.00010
0.00005
0.00000
Surface.Detritus
0.00020
0.00015
0.00010
0.00005
0.00000
Meso.Detritus
7e−05
6e−05
5e−05
4e−05
3e−05
2e−05
1e−05
0e+00
Deepwater.Detritus
1e−04
8e−05
6e−05
4e−05
2e−05
0e+00
5
10
15
20

As Australia’s national science agency, CSIRO is solving the greatest challenges through innovative science and technology.

Contact us

1300 363 400
+61 3 9545 2176
csiro.au/contact
csiro.au

For further information

CSIRO Environment
Dr Piers Dunstan
+61 3 6232 5382
piers.dunstan@csiro.au
research.csiro.au/dsm